Understanding Sulfur Poisoning of Bimetallic Pd-Pt Methane Oxidation Catalysts and their Regeneration

Patrick Lott[a], Mario Eck[a], Dmitry E. Doronkin[a,b], Anna Zimina[b], Steffen Tischer[b], Radian Popescu[c], Stéphanie Belin[d], Valérie Briois[d], Maria Casapu[a], Jan-Dierk Grunwaldt[a,b,*], Olaf Deutschmann[a,b,*]

[a] Institute for Chemical Technology and Polymer Chemistry (ITCP), Karlsruhe Institute of Technology (KIT), Engesserstr. 20, 76131 Karlsruhe, Germany

[b] Institute of Catalysis Research and Technology (IKFT), Karlsruhe Institute of Technology (KIT), Hermann-von-Helmholtz Platz 1, 76344 Eggenstein-Leopoldshafen, Germany

[c] Laboratory for Electron Microscopy (LEM), Karlsruhe Institute of Technology (KIT), Engesserstr. 7, 76131 Karlsruhe, Germany

[d] Synchrotron SOLEIL, L'Orme des Merisiers - St. Aubin, BP 48, 91192 Gif-sur-Yvette Cedex, France

* Jan-Dierk Grunwaldt: grunwaldt@kit.edu

* Olaf Deutschmann: deutschmann@kit.edu

Abstract

$Pd-Pt/Al_2O_3$ and $Pd-Pt/CeO_2-ZrO_2-Y_2O_3-La_2O_3$ methane oxidation catalysts were investigated under typical lean-burn gas engine conditions with respect to sulfur poisoning and during reactivation, particularly under the most efficient rich conditions. Sulfation of the noble metal and the support material led to pronounced catalyst deactivation. A pronounced transfer of sulfates to the support, particularly alumina, only partially protects the noble metal. *In situ* X-ray absorption spectroscopy gave insight into the nature and evolution of Pd species during regenerative treatment. Although palladium sulfate that formed during poisoning is decomposed at approximately 200°C in oxygen-free conditions, support regeneration requires higher temperatures, which result in PdS formation above 400°C. Despite its high stability under rich conditions, PdS decomposition by oxidation in lean atmosphere leads to the recovery of the activity. In addition, water vapor that is present during the rich regeneration exhibited a beneficial effect on the regeneration with higher catalytic activity after regeneration.

1. Introduction

Due to high fuel efficiency, comparatively low CO_2 emissions and rather low costs, lean-burn engines powered by conventional natural gas, biogas or gas originating from power-to-gas processes are of great interest. In the mobile sector these engines can be utilized in the so-called Natural Gas Vehicles (NGVs) or in marine ships while application in stationary power plants is widespread for energy production. Despite the many advantages, incomplete combustion is the main obstacle that currently impedes a more intense use of natural gas engines. The main component of natural gas, methane, has a more than 20 times higher greenhouse potential compared to CO_2 and thus acts as a strong greenhouse gas if emitted into the atmosphere [1]. Hence, emission legislation becomes more stringent, making an effective exhaust gas after-treatment system mandatory that is particularly capable of converting CH_4 as most stable molecule among all alkanes [2, 3]. Although palladium catalysts show the highest activity for the total oxidation of methane at low temperatures [4, 5], they strongly benefit from moderate platinum addition. These bimetallic Pd-Pt catalysts exhibit less inhibition of the methane oxidation reaction that is caused by the inevitable exhaust gas component water [6-9] and a reduced noble metal particle sintering tendency [10-13]. While it is widely accepted that PdO or at least PdO_x-PdO composites are the most active phase during total oxidation of methane [14-23], the role of the support material is still under debate. In contrast to Al_2O_3, the use of CeO_2-ZrO_2 is often motivated by the strong noble metal-support interactions and the beneficial high oxygen mobility of the reducible support [24, 25].

The main challenge of Pd-Pt catalysts remains the strong poisoning by sulfur containing compounds such as SO_2 or H_2S [26]. Sulfur compounds typically originate either from the gaseous fuel itself or odorants added to the natural gas, but are also formed from lubricants used

in the engine. Palladium and especially platinum can easily oxidize sulfur compounds to SO_3 and H_2SO_4 [27], leading to the formation of stable and catalytically inactive $PdSO_4$, as unraveled by infrared (IR) spectroscopy [28, 29] and X-ray photoelectron spectroscopy (XPS) [30]. Moreover, the formation of rather stable surface sulfites/sulfates on support materials such as Al_2O_3, CeO_2, ZrO_2 or their mixed oxides was observed [31-36]. According to Sadokhina et al. [37] the presence of NOx in the reaction gas mixture lowers sulfate formation and favors surface sulfite formation on a $Pt-Pd/Al_2O_3$ catalyst. Furthermore, they reported a delay in deactivation by the presence of NOx, an effect that is most pronounced at high temperatures (550°C). Also a careful choice of the support material can slow down the poisoning process. Alumina, for instance, is known to store significant amounts of sulfates, which temporarily protects the noble metal [36-39]. In contrast, non-sulfating supports such as ZrO_2-SiO_2 show no significant uptake of sulfur species resulting in faster deactivation, but can be faster regenerated, as no spillover back to the noble metal particles takes place [38]. Similarly, doping alumina with Ti and Si, both forming less sulfates than alumina [40-42], facilitates desorption of sulfur species and can hereby ease the regeneration [43]. With respect to regeneration, rich conditions are well known to facilitate the removal of the sulfur compounds [44-48]. In fact, we recently demonstrated the effectiveness of a pulse-like rich treatment to stabilize the catalytic activity during real engine operation [49]. Nevertheless, at moderate temperatures (around 500-550°C) no full regeneration can be achieved for alumina-supported catalysts. This seems to be due to remaining $Al_2(SO_4)_3$ species that re-poison the noble metal particles as reported by Honkanen et al. [50]. Such an effect has not been observed for a CeO_2-ZrO_2 support [49].

Moreover, also noble metal properties such as particle size, structure or alloying significantly influence the sulfur poisoning and regeneration behavior. Wilburn and Epling [51-54] reported

that, e.g., the amount of adsorbed SO_2 decreases with increasing particle size [51]. Furthermore, the evaluation of the Pd:Pt molar ratio revealed that aluminum sulfate formation is favored for Pd-rich catalysts at low temperatures (100°C) and the efficiency to regenerate SO_2-poisoned catalysts via temperature programmed reduction (TPR) or desorption (TPD) decreases with increasing Pt content [52, 53]. The crucial role of the noble metal state during regenerative treatment was also highlighted by Nissinen et al. [55], who investigated a $PdSO_4/Al_2O_3$ model catalyst by means of powder X-ray diffraction (XRD). Application of a H_2-containing atmosphere resulted in Pd_4S-formation. Similarly, in one of our recent *operando* X-ray absorption spectroscopy (XAS) study we found PdS formation during dynamic lean-rich catalyst operation in presence of SO_2 [56].

However, there is still a strong debate on the molecular processes occurring during reactivation under rich conditions, on the role of Pt and Pd during poisoning and regeneration and the role of the support. In the present study, we aim at a fundamental understanding of the SO_2 poisoning of bimetallic $Pd-Pt/Al_2O_3$ and $Pd-Pt/CeO_2-ZrO_2-Y_2O_3-La_2O_3$ catalysts. The effects of catalyst support, poisoning temperature and regeneration conditions are investigated by systematic activity tests and a comprehensive characterization. Particularly, the state of the noble metals of the as-prepared and poisoned catalysts and its evolution during catalyst regeneration is elucidated by *ex situ*/*in situ* X-ray absorption spectroscopy (XAS) at the Pd K- and Pt L_3-edges. To our knowledge, this is the first study to directly follow the state of the noble metal *in situ* during regeneration under selected conditions, which allows to unravel the role of the gas mixture and catalyst composition on the regeneration behavior. This information is mandatory for designing efficient catalyst regeneration procedures that allow a long-term application of methane oxidation catalysts in the future.

2. Experimental

2.1 Catalyst Preparation

A 2.4 wt.% Pd-Pt/CeO_2-ZrO_2-Y_2O_3-La_2O_3 and a 2.4 wt.% Pd-Pt/γ-Al_2O_3 sample (Pd:Pt 5:1 weight ratio) were prepared by incipient wetness impregnation of commercial CeO_2-ZrO_2-Y_2O_3-La_2O_3 mixed oxide (Interkat, metal weight ratios 30:60:5:5; as ceria and zirconia are the main components in the following referred to as CZ for reasons of better readability) and commercial γ-Al_2O_3 (SASOL), respectively. Both materials were calcined at 700°C for 5 h in static air prior to the synthesis. Afterwards, an aqueous solution of tetraamminepalladium(II) nitrate (ChemPUR, 3.3 wt.% aqueous solution) and tetraammineplatinum(II) nitrate (VWR, purity > 99.9%) was used for the impregnation of the supports. To obtain the desired noble metal loading of 2.4 wt.%, two impregnation steps with 5 h of drying at room temperature (RT) and 1 h at 70°C in between were necessary for the CZ mixed oxide. The catalyst samples were prepared with a robot-controlled preparation unit [57, 58] (Accelerator SLT106 Parallel Synthesizer – SLT CATIMPREG, ChemSpeed Technologies). After the final impregnation step and drying at 70°C for 12 h, the resulting samples were calcined in static air at 550°C for 5 h.

2.2 Catalyst Characterization

A BELSORP Mini II analyzer (MicrotracBEL) was used to estimate the surface area and the total pore volume according to the Brunauer-Emmet-Teller (BET) method [59] by measuring N_2 physisorption at – 196°C. Prior to the analysis, the samples were degassed at 300°C for 2 h.

X-ray diffraction (XRD) patterns were collected in step scanning regime from 20° to 90° with a step size of $\Delta(2\theta) = 0.016°$ (0.51 s/step dwell time) using a Bruker Advance D8 diffractometer with Cu Kα radiation (wavelength $\lambda = 0.154$ nm).

A temperature programmed desorption of sulfur containing species (S-TPD) was performed by heating 300 mg of previously poisoned catalyst sample diluted with 700 mg of SiO_2 with 5°C/min from RT to 900°C in 1 L/min N_2 (dosed via Bronkhorst mass flow controllers) and keeping them at this temperature for 5 min. Desorbed SO_2 was monitored by a Fourier-transform infrared spectrometer (FTIR, MultiGas MG2030, MKS). Since inert conditions do not result in SO_3 evolution [49], only SO_2 desorption profiles are reported.

To investigate the size and the chemical composition of the Pd-Pt nanoparticles as well as the distribution of sulfur on the catalyst after aging, a combination of high-angle annular dark-field (HAADF) scanning transmission electron microscopy (STEM) and energy-dispersive X-ray spectroscopy (EDXS) was used. Samples were prepared at RT in air by drop-casting of the fine catalyst powder dispersed in ethanol onto a commercial holey ultrathin amorphous carbon film (3 nm) mounted on a 400 µm mesh Cu grid (Plano 01824). The study was performed with an FEI OSIRIS ChemiSTEM microscope at 200 kV electron acceleration voltage equipped with a Bruker Quantax system (XFlash detector). EDX spectra are quantified with the FEI software package "TEM imaging and analysis" (TIA) version 4.7 SP3. By using TIA element concentrations were calculated on the basis of a refined Kramers' law model that included corrections for detector absorption and background subtraction. The concentration profiles of Pd and Pt within single nanoparticles were determined by quantification of their EDXS drift-corrected spectra recorded along a line-scan that passes through their center. Hereby, the Pd-L and Pt-L series were used. EDX spectra obtained during scanning of a rectangular area within single nanoparticles are used to determine their average chemical composition. Additionally, EDXS elemental maps of Pd (Pd-$L_{\alpha1}$ line), Pt (Pt-$L_{\alpha1}$ line) and S (S-$K_{\alpha1}$ line) are recorded and

used to investigate their distribution within a Pd-Pt particle. The maps are analyzed by using the Bruker software package ESPRIT (version 1.9).

A more detailed analysis of the sulfur species formed during different aging treatment was done with *ex situ* diffuse reflectance infrared spectroscopy (DRIFTS) using a Bruker Vertex 70 system equipped with a Harrick Praying Mantis DRIFTS cell. The catalyst samples were exposed to the SO_2 containing gas atmosphere for 15 h and then transferred to the DRIFTS cell without any further pre-treatment. Difference spectra between fresh and aged catalyst samples were finally used to investigate the formed species.

2.3 Tests on Catalyst Test Bench

General procedure: For the powdered catalysts, a bed of 1.5 cm fixed by quartz glass wool was obtained by diluting 300 mg of catalyst sample (125 – 250 μm sieve fraction) with 700 mg quartz sand (125 – 250 μm) and placing this mixture in a quartz glass tubular reactor (8 mm i.d.). For all tests, the temperature was monitored by two thermocouples placed approximately 5 mm upstream and downstream of the catalyst bed. Reactor heating and cooling was controlled by Eurotherm controllers using the thermocouple located upstream of the catalyst bed. The reaction gases were dosed by Bronkhorst mass flow controllers (MFC) while water was dosed via a controlled evaporator mixer (CEM, Bronkhorst). Finally, all reaction products were monitored by an FTIR spectrometer (MultiGas 2030, MKS).

Deactivation in SO_2 containing atmospheres: For every test a fresh sample was used and degreened at 550°C in 3200 ppm CH_4, 10% O_2 in N_2 for 1 h prior to each run. The GHSV for these experiments was kept constant at 80 000 h^{-1}. Deactivation experiments were performed at three different temperatures (400°C, 450°C and 500°C) and with an SO_2 concentration of 5 ppm.

A typical experiment consisted of the following sequence (for details see Figures S1 and S2 in the supporting information):

(i) a light-off/light-out experiment in the fresh state between 225°C and 550°C (3°C/min) using the SO_2-free reaction mixture containing 3200 ppm CH_4, 10% O_2 and 12% H_2O in N_2;

(ii) 15 h of sulfur poisoning at 400°C, 450°C or 500°C in 3200 ppm CH_4, 10% O_2, 12% H_2O and 5 ppm SO_2 in N_2 (The sulfation was completed after 15 h of aging, since the dosed SO_2 amount could be detected at the reactor outlet, which clearly evidences no further sulfur uptake after the poisoning period and hence a completely sulfated sample.);

(iii) a second light-off/light-out cycle up to 550°C in the above mentioned SO_2-free reaction mixture;

(iv, a) a temperature programmed desorption (TPD) or reduction (TPR) by heating the samples with 5°C/min from RT to 900°C in N_2 ("inert") or 3200 ppm CH_4 in N_2 ("rich") and keeping them at this temperature for 5 min;

(iv, b) or a temperature programmed reduction (TPR) by heating the samples with 5°C/min from RT to 750°C in 3200 ppm CH_4 and N_2 ("rich") and keeping them at this temperature for 5 min followed by a third light-off/light-out cycle up to 550°C in the SO_2-free reaction mixture. (A cross-sensitivity in the FTIR analyzer between CH_4, H_2O and SO_2 impedes precise SO_2 quantification during aging, thus, no reliable sulfur balance as comparison between adsorbed and desorbed SO_2 can be given.)

2.4 XAS Measurements

General procedure: Ex situ analysis was performed at the CAT-ACT beamline [60] (KIT synchrotron, Karlsruhe, Germany) at the Pd K-edge (24 350 eV) using a Si(311) double crystal monochromator (DCM). Pellets of fresh and aged catalyst diluted with cellulose were measured

in transmission geometry. Measurements at the S K-edge (2472 eV) were conducted in fluorescence mode at the SUL-X beamline [61] (KIT synchrotron, Karlsruhe, Germany) using a Si(111) monochromator and a 7 element Si(Li) fluorescence detector (Gresham, now RaySpec Ltd). Time-resolved *in situ* XAS measurements were primarily conducted at the ROCK beamline [62] (SOLEIL, Saint-Aubin, France) in transmission mode, while alternating between the Pd K-edge (24 350 eV) and the Pt L_3-edge (11 564 eV), using Si(220) and Si(111) DCMs, respectively. The obtained results were validated and extended at the SAMBA beamline [63] in fluorescence mode (SOLEIL, Saint-Aubin, France) and at the P64 beamline [64] (DESY/PETRA III, Hamburg, Germany) in transmission mode using a Si(311) DCM. Both beamlines, ROCK and P64, are dedicated to study fast kinetic processes during catalytic reactions. In addition, the ROCK beamline allows to measure alternately at two edges, which is particularly relevant in our experiments with bimetallic Pd-Pt catalysts.

Experimental setup: For the *in situ* experiments, the catalyst samples were placed in quartz capillary microreactors (diameter 1.5 mm, wall thickness 0.02 mm) between two quartz glass wool plugs. Heating was realized using a hot gas blower system (GSB-1300, FMB Oxford) [16] while the gas mixture into the reactor was fed by Bronkhorst MFCs and water was dosed via a saturator.

Regeneration of SO_2 poisoned catalyst samples: Samples of Pd-Pt/Al_2O_3 and Pd-Pt/CZ were deactivated at 450°C in the reaction gas mixture containing 5 ppm SO_2, 3200 ppm CH_4, 10% O_2, 12% H_2O and balance N_2 at a gas flow of 1 L/min for 15 h at the lab bench in a continuous flow reactor. The poisoned catalysts were placed in the quartz capillary microreactors and temperature programmed experiments in different gas mixtures (Table 1) were performed in order to regenerate the sulfur poisoned catalysts.

Table 1. Gas mixtures during the temperature programmed experiments monitored by *in situ* XAS.

Gas mixture (GM) no.	O_2 [%]	H_2O [%]	CH_4 [%]	He [%]
1 – TPD	0	0	0	100
2 – RM	10.0	1.50	0.32	88.18
3 – CH_4-TPR (dry)	0	0	0.32	99.68
4 – CH_4-TPR (wet)	0	1.50	0.32	98.18

Data evaluation: The obtained X-ray absorption spectra were evaluated using ATHENA and ARTEMIS from the IFFEFIT software package [65]. Quantification of noble metal species, e.g. palladium as oxidized, reduced, sulfide or sulfate species, was conducted by linear combination fitting (LCF) of normalized X-ray absorption near edge spectra (XANES) with spectra of reference compounds for palladium (PdO for oxidized unpoisoned species, reduced Pd nanoparticles, $PdSO_4$, $PdSO_4 \cdot 2\ H_2O$, PdS, typically limited to a maximum of 3 components) in the range 24 345 – 24 420 eV and for platinum (metallic Pt and PtO_2) in the range 11 545 – 11 605 eV. For metallic (reduced) Pd nanoparticles a reference spectrum was obtained from a fully reduced Pd-Pt catalyst, as the XAS spectra of Pd nanoparticles slightly differ from bulk-like palladium foil and also may be influenced by alloy formation with platinum. In this context, the Fourier-transformed extended X-ray absorption fine structure (FT-EXAFS; k^2-weighted EXAFS data; k-range 2.5 – 14 $Å^{-1}$ for the reference spectra, k-range 3 – 12 $Å^{-1}$ for the sample spectra) spectra show weaker backscattering due to a lower average number of nearest neighbors compared to the bulk metal [66]. As decomposition and stability data of Pt-S compounds point to

irrelevancy for the conditions investigated in the present study [67, 68], no sulfur containing platinum references were considered in this study.

3. Results and Discussion

3.1 Catalyst Characterization of Fresh and Sulfur-Poisoned Catalysts

After incipient wetness impregnation, N_2-physisorption revealed a BET surface area of 180 m^2/g for the Pd-Pt/Al_2O_3 catalyst and of 75 m^2/g for Pd-Pt/CZ. Furthermore, the catalysts' target noble metal loading of about 2.0 wt.% Pd and 0.4 wt.% Pt was confirmed by elemental analysis via inductively coupled plasma optical emission spectrometry (ICP-OES, cf. Table S1). The XRD patterns of the fresh and SO_2-poisoned bimetallic powdered catalysts and the pure support materials are displayed in Figure 1. The reflections of Al_2O_3 at 32°, 38° and 40° as well as the reflections of CeO_2-ZrO_2 mixed oxide at 29° and 34° become broader with increasing aging temperature. This indicates structural changes of the support material during sulfur aging at elevated temperatures, e.g. due to bulk sulfation. Only small reflections originating from PdO or Pd were found for the freshly impregnated samples on alumina at $2\theta = 34°$ and 55°, whereas on CZ no noble metal related reflections were found in the fresh state. This indicates either high dispersion of the noble metal particles on the support or low crystallinity. However, pronounced reflections at $2\theta = 34°$, 55° and 72° were detected for all SO_2-poisoned Al_2O_3-based catalysts, which indicates the formation of larger (bimetallic) Pd and Pt particles induced by sintering. The reflections from metallic Pd ($2\theta = 40°$, 47°, 68° and 82°) could not be observed for any sample, which might be due to an overlap with reflections of the support material or due to the fact, that only PdO is present.
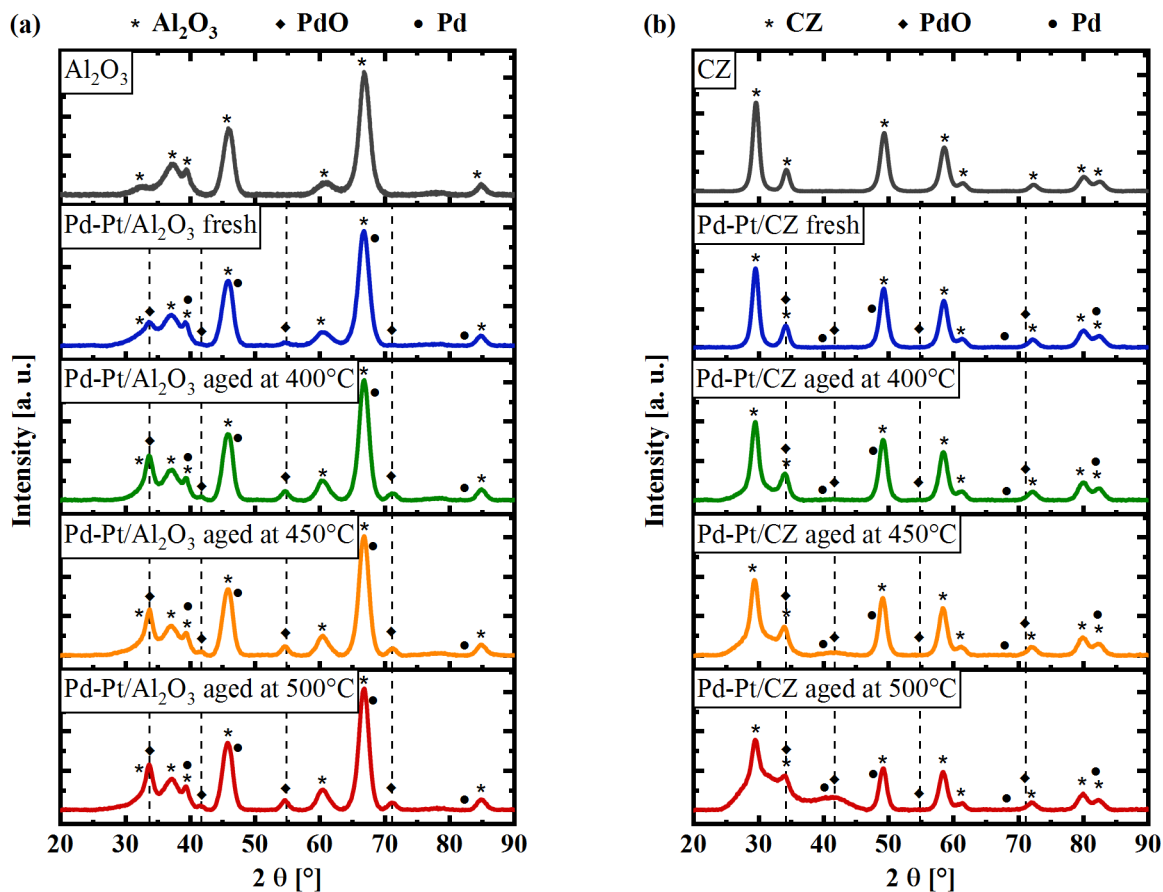
Figure 1. XRD patterns of (a) Pd-Pt/Al$_2$O$_3$ and (b) Pd-Pt/CZ catalysts.

HAADF STEM images of the fresh (as prepared) catalyst sample revealed a mean noble metal particle diameter of d$_{mean}$ = 4.5 ± 1.5 nm for Pd-Pt/Al$_2$O$_3$ (Figure 2a), while EDXS scans show that Pd and Pt supported on Al$_2$O$_3$ form homogeneously alloyed nanoparticles with an average composition of Pd$_{93±4}$Pt$_{7±4}$ (averaged over about 200 nanoparticles). In good accordance with the XRD data (Figure 1), the transmission electron microscopy (TEM) reveals particle sintering induced by SO$_2$ poisoning at 500°C. After exposure to the reaction environment, Pd-Pt alloyed nanoparticles are found on the alumina support (Figure S3), characterized by a larger mean particle diameter of approximately d$_{mean}$ = 6.5 ± 2.5 nm (Figure 2b). EDXS maps of palladium and sulfur on the poisoned Pd-Pt/Al$_2$O$_3$ catalyst show that almost all noble metal nanoparticles

13

and also the Al_2O_3 substrate are contaminated with sulfur (Figure S3). Small nanoparticles of about 2 nm in diameter contain up to 20 at.% S, whereas the sulfur level decreases to 2 at.% for the larger Pd-Pt nanoparticles (Figure S4). These findings indicate that only surface poisoning and no bulk poisoning occurs for larger noble metal particles. A similar observation was reported by Wilburn and Epling [51] who described a particle size dependency of sulfur poisoning.

With an average diameter of $d_{mean} = 5.3 \pm 2.8$ nm the fresh Pd-Pt/CZ catalyst exhibits slightly larger particles than the corresponding alumina-supported sample (Figure 2c). Also on the CZ-support the particles consist mainly of a bimetallic Pd-Pt alloy with an average composition of $Pd_{94\pm2}Pt_{6\pm1}$. Additionally, highly dispersed Pt species (< 1 nm) were found on the CZ substrate, which are, however, not considered in the histogram shown in Figure 2c, where only bimetallic particles were counted. These small Pt particles probably originate from the strong interactions between Pt and CeO_2 [58, 69], possibly causing Pt segregation out of the Pd-Pt-particles during catalyst calcination. Sulfur aging at 500°C resulted in a mean particle size of $d_{mean} = 6.3 \pm 2.8$ nm for Pd-Pt/CZ (Figure 2d), which again indicates a slight sintering of the bimetallic particles. Aside, the monometallic highly dispersed Pt particles on CZ were also observed after the aging. As the weak S-K_α line (2309 eV) is located on the tail of the strong Zr-L_α (2044 eV) and Zr-L_β (2125 eV) lines, the sulfur contamination of Pd-Pt/CZ could not be accurately investigated by means of EDXS. Nonetheless, it has been previously claimed that a similar poisoning of particles and support occurs, as CeO_2 and ceria-zirconia mixed oxides are known to form sulfates [32, 33]. This suggestion is also supported by the results obtained during TPD/CH_4-TPR, XAS and DRIFTS experiments, which are presented in the following.
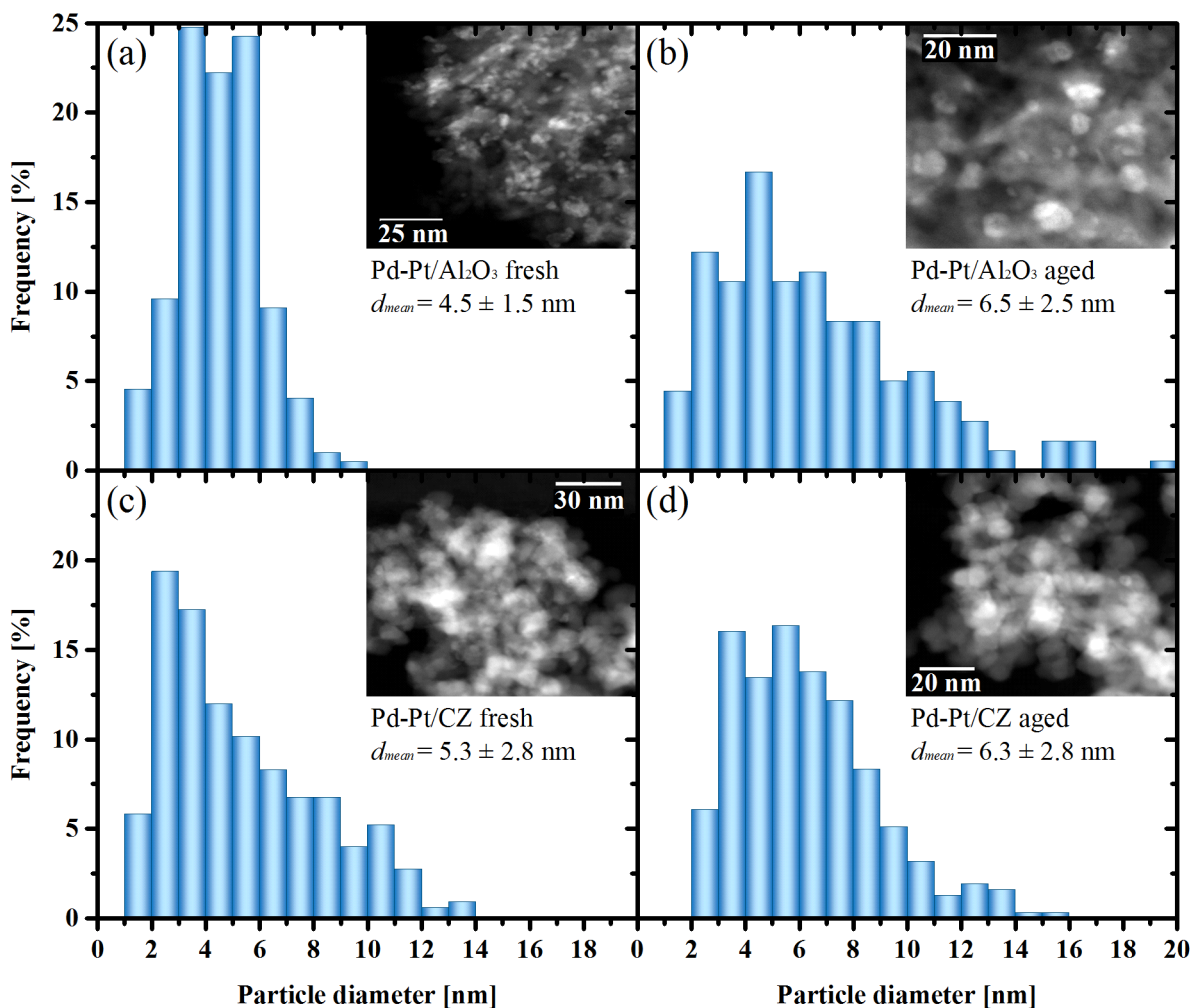
Figure 2. Typical HAADF STEM images and corresponding particle size distributions calculated based on the analysis of approximately 200 Pd-Pt particles located on many HAADF STEM images recorded at different magnifications: (a) Pd-Pt/Al$_2$O$_3$ and (c) Pd-Pt/CZ in the fresh state; (b) Pd-Pt/Al$_2$O$_3$ and (d) Pd-Pt/CZ after aging in the presence of SO$_2$ at 500°C for 15 h.

Reference materials, fresh catalyst samples and samples poisoned with SO$_2$ were investigated by means of XAS. The Pd K-edge spectra of the reference materials PdO, PdS, PdSO$_4$, PdSO$_4$ · 2 H$_2$O, Pd foil and reduced Pd nanoparticles are shown in Figure 3 and those for the catalysts in Figure 4. The XANES spectra of the aged Pd-Pt/Al$_2$O$_3$ and Pd-Pt/CZ samples

strongly resemble the spectra of the fresh catalysts, indicating a similar oxidation state (Pd^{2+}) after the aging. However, the slight differences might be explained by surface sulfation. The comparison of the extended X-ray absorption fine structure (EXAFS) for the Pd-Pt/Al$_2$O$_3$ catalyst samples reveals a slight sintering after aging as the second shell contribution to the FT increases (Figure 4b), while no noteworthy differences can be observed between the samples aged at different temperatures. Although the signal-to-noise ratio is worse for the Pd-Pt/CZ samples due to presence of highly absorbing Zr and Ce, a similar observation is made for Pd-Pt/CZ after aging. However, the increase of the second shell signal is lower (Figure 4d), which points to less sintering on CZ compared to the alumina-supported samples. This is in good accordance with the corresponding TEM images, which revealed an increase of the mean noble metal particle diameter from 4.5 nm to 6.5 nm on alumina and from 5.3 nm to 6.3 nm on the CZ support (Figure 2) due to SO$_2$ poisoning at 500°C for 15 h.
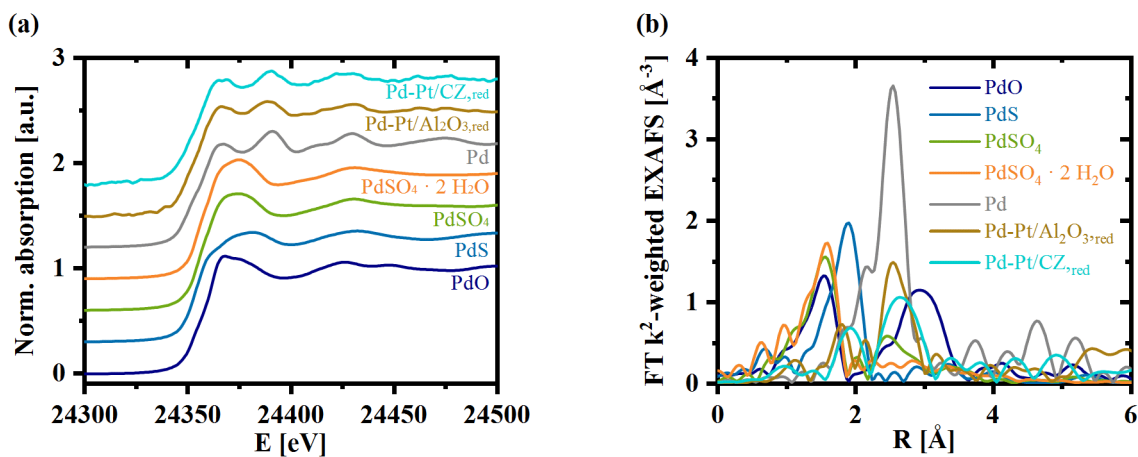
Figure 3. (a) Pd reference spectra used for linear combination fitting (LCF) of the XANES region and (b) the Fourier-transformed k^2-weighted EXAFS data (k-range 2.5 - 14 Å^{-1}, uncorrected for the phase shift) vs. radial distance. The data for Pd foil are shown for the reader's convenience, however, fully reduced Pd nanoparticle spectra were used for the LCF analysis (Pd-Pt/Al$_2$O$_{3,red}$ and Pd-Pt/CZ$_{,red}$).
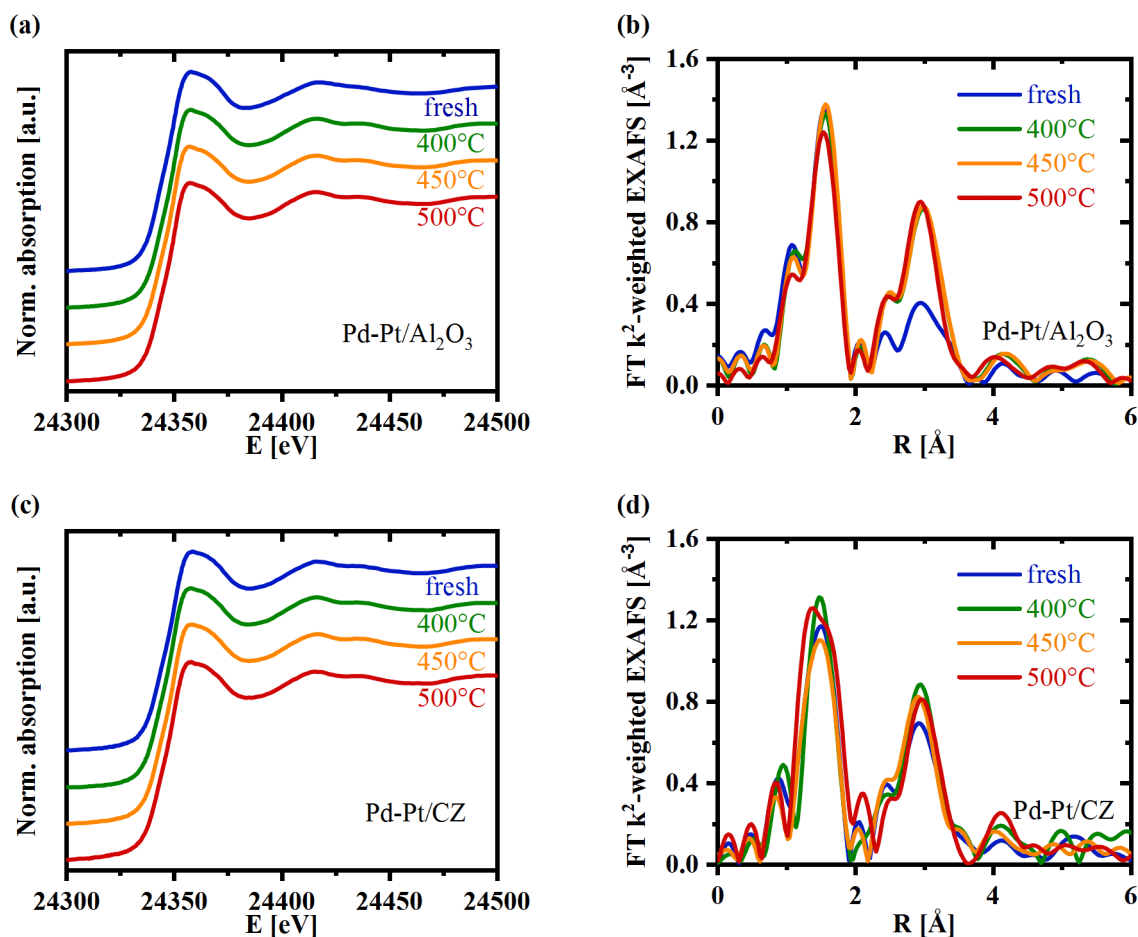
Figure 4. *Ex situ* XANES spectra and Fourier-transformed k^2-weighted EXAFS (k-range 3 - 12 Å^{-1}, uncorrected for the phase shift) vs. radial distance of (a, b) Pd-Pt/Al$_2$O$_3$ and (c, d) Pt-Pt/CZ as fresh samples and after sulfur aging for 15 h at 400°C, 450°C and 500°C in 3200 ppm CH$_4$, 10% O$_2$, 12% H$_2$O, 5 ppm SO$_2$ in N$_2$.

A more comprehensive knowledge of the formed sulfur species can be obtained by considering S K-edge XANES spectra of the poisoned catalyst samples and of several reference compounds. The sulfur K-edge has been assigned to the dipole-allowed transitions from a 1s core orbital to an unoccupied p-orbital in the sulfur atom, more precisely, to a sp^3-hybridized state between O and S or to a sp-bond between Pd and S. Therefore, profile, position and intensity of the S K-edge spectrum is directly dependent on the number and type of its first neighbors [70-72], making

such measurements highly sensitive to oxidation state, orbital mixing and bonding. In the present study analysis was conducted by comparison to reference compounds (Figure 5, Figure S5 and Table S2).

The spectra of the poisoned Pd-Pt/Al_2O_3 catalysts show a pronounced S K-edge jump (Figure 5a) that resembles very well the $Al_2(SO_4)_3$ spectrum (absorption edge at 2480.9 eV), confirming the S^{6+} oxidation state for sulfur (SO_4^{2-}) [70]. Sulfide species (S^{2-}) as encountered for PdS, on the other hand, are typically shifted by about 10 eV, as can be seen in Figure 5, and are not observed in the sample spectra. $PdSO_4 \cdot 2\,H_2O$ and $PdSO_4$ show a slight pre-edge peak, which appears due to the electron transition from the sulfur 1s orbital to the mixed orbitals of S 3p and unoccupied Pd d orbitals [70]. No pronounced variation was recognized when comparing the XANES spectra of the catalysts poisoned at different temperatures. In line with literature [28, 29, 31, 36] the obtained S K-edge XANES spectra indicate the formation of sulfates during poisoning in the presence of SO_2, O_2 and H_2O at temperatures between 400°C and 500°C. However, the data do not allow a clear distinction between noble metal and support-related sulfates, making additional investigations mandatory. Moreover, the low Pd content makes it difficult to accurately conclude on the state of noble metal sites solely based on the S K-edge measurements. The characteristic pre-edge peak of palladium sulfate dehydrate at 2478 eV, for instance, is hardly visible in the sample spectra.

Also for the samples supported on CZ the characteristic S absorption edge around 2480 eV uncovers the formation of sulfates. Although the profile of the XANES spectra does not resemble that of pure cerium or zirconium sulfate, the shape of the whiteline is asymmetric for the sulfur-poisoned samples. This strongly suggests a contribution of support-related sulfates to the XANES spectra, since the whitelines of $ZrSO_4$ and $CeSO_4$ are also asymmetric. The position

of the pre-edge feature at 2477 eV that most likely originates from $CeSO_4$ supports this assumption, whereas the low loading with noble metal species does not allow to clearly prove $PdSO_4$ formation. The differences observed between reference compounds and sample spectra could be due to the different electronic properties and also the existence of various S-species on Y-La-doped CZ.
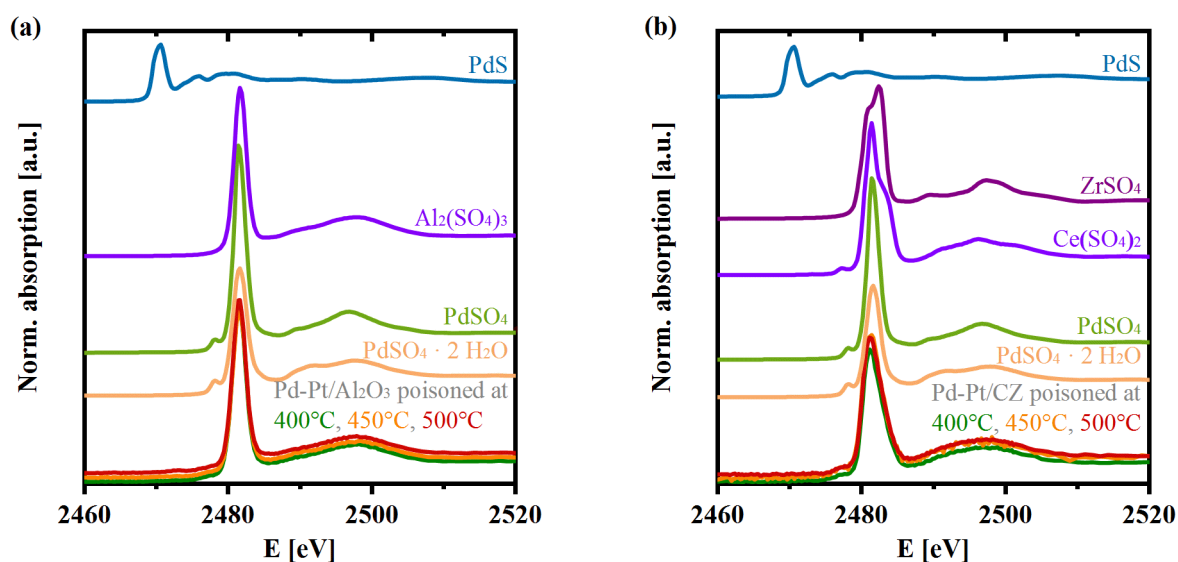
Figure 5. XANES spectra obtained by measurements at the S K-edge for the sulfur poisoned samples (poisoning at 400°C, 450°C and 500°C) and the reference substances $Al_2(SO_4)_3$, $Ce(SO_4)_2$, $ZrSO_4$, $PdSO_4$, $PdSO_4 \cdot 2\ H_2O$ and PdS.

3.2 Catalytic Performance and Influence of Temperature on Deactivation in SO_2-containing Model Gas

Irrespective of the poisoning temperature the addition of 5 ppm SO_2 to the gas stream led to an instant and rapid drop in methane oxidation activity, resulting in a pronounced deactivation of the catalyst within only few hours (Figure 6). At low temperatures the deactivation is faster for both catalysts, which supports one of our recent studies [49]. The activity loss originates from the poisoning of the active Pd species, i.e. by formation of surface and bulk-like $PdSO_4$ [29, 38].

Such a process involves oxidation of SO_2 to SO_3 and H_2SO_4, especially favored by the presence of Pt [27, 73]. Moreover, also the support material can store sulfites/sulfates. Alumina for instance is known to form bulk $Al_2(SO_4)_3$ to large extent [36], but also ceria and ceria-zirconia mixed oxides are reported to form both, surface- and bulk-related sulfates [32, 33]. As the noble metal particle size increased only by ~1-2 nm (Figure 2) during the aging at 500°C, the changes in activity cannot be explained by particle sintering but are mainly caused by the SO_2 poisoning. While Pd-Pt/Al_2O_3 remains slightly active after poisoning at 450°C and 500°C for 15 h and reaches a steady state of ~7% conversion and ~32% conversion (Figure 6a), respectively, Pd-Pt/CZ shows almost no catalytic activity after the SO_2-aging (Figure 6b). This points to a different poisoning mechanism, most probably influenced by the different support materials.
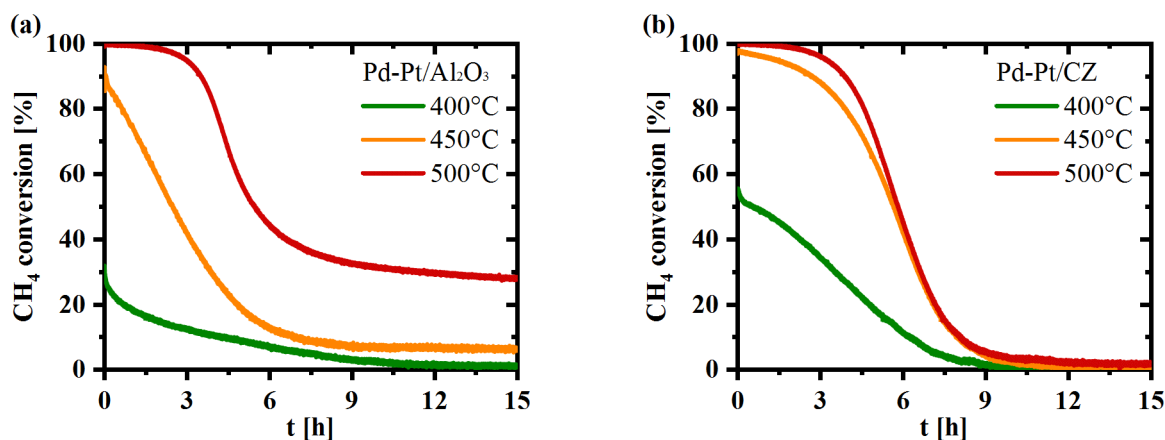
Figure 6. CH_4 conversion as function of time on stream over (a) Pd-Pt/Al_2O_3 and (b) Pt-Pt/CZ at 400°C, 450°C and 500°C. Gas composition: 3200 ppm CH_4, 10% O_2, 12% H_2O, 5 ppm SO_2 in N_2. GHSV = 80 000 h^{-1}.

Pronounced deactivation due to sulfur poisoning is also visible during the light-off activity tests. In the fresh state, both catalysts, Pd-Pt/Al_2O_3 (Figure 7a) and Pd-Pt/CZ (Figure 7b), show the typical methane conversion profiles for such catalysts [49, 74] with a T_{50} (temperature of 50% methane conversion) of about 400°C in a steam containing gas atmosphere. SO_2-poisoning

at 400°C for 15 h resulted in an increase of T_{50} by 88°C for Pd-Pt/Al$_2$O$_3$; an increasing poisoning temperature shifts T_{50} to even higher temperatures (Figure 7a). The catalyst aged at 400°C still shows full conversion at 550°C whereas the maximum conversion for the sample aged at 500°C is only ~90% at 550°C. A slightly higher activity of Pd-Pt/Al$_2$O$_3$ was measured during each light-out (inverse hysteresis, Figure S7), which is due to a SO$_2$ release during the light-off that starts at around 450°C and indicates a minor *in situ* regeneration of the catalyst in the SO$_2$-free reaction gas mixture. However, during the light-off less SO$_2$ was desorbed for the samples aged at higher temperature, resulting in a less pronounced inverse hysteresis. This might be explained by predominant formation of surface sulfite and sulfate species at low temperatures (400°C) [36], whereas at higher temperatures more pronounced bulk sulfation takes place. As the decomposition of bulk-like species is slower, they are probably more difficult to decompose during the light-off and thus keep the catalyst poisoned.

The more pronounced deactivation of the CZ-supported sample observed during the SO$_2$-aging is also visible during the subsequent light-off (Figure 7b). Irrespective of the aging temperature, the catalyst supported on ceria-zirconia does not show more than 10% conversion after SO$_2$-poisoning at the maximum light-off temperature of 550°C.
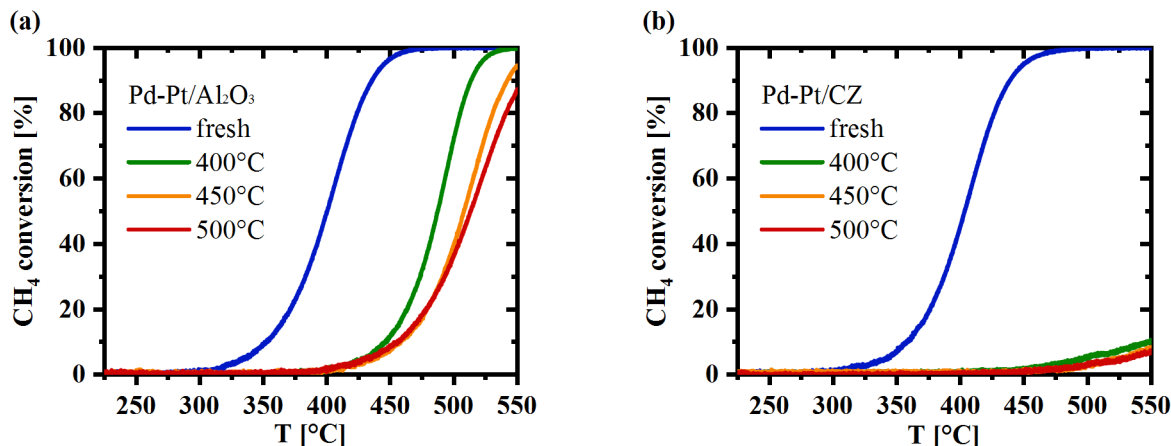
Figure 7. Light-off curves for (a) Pd-Pt/Al$_2$O$_3$ and (b) Pd-Pt/CZ before ("fresh") and after SO$_2$-poisoning at 400°C, 450°C and 500°C; gas composition during the activity test: 3200 ppm CH$_4$, 10% O$_2$, 12% H$_2$O in N$_2$. GHSV = 80 000 h^{-1}.

3.3 The Influence of Temperature during Sulfur Poisoning on the Formed Species

In consideration of the different activity trends presented above we can speculate that the aging temperature and the choice of the support material leads to formation of different species on the catalyst. To verify this hypothesis, SO$_2$-poisoned Pd-Pt/Al$_2$O$_3$ and Pd-Pt/CZ samples were studied by complementary *ex situ* DRIFTS experiments. Figure 8 shows the DRIFTS spectra obtained after exposure to the sulfur containing reaction gas mixture in comparison to the freshly prepared and calcined catalyst (difference spectra). Raw difference reflectance spectra can be found in the supporting information (Figure S6). After aging at 400°C, Pd-Pt/Al$_2$O$_3$ shows an extremely weak band in the region 1000 to 950 cm^{-1}, which is characteristic for aluminum surface sulfites [75, 76]. A broad intense band is observed at ~1500 cm^{-1}, which might be attributed to carbonate species [77, 78]. Although methane oxidation over monometallic PdO catalysts presumably proceeds via formates and not carbonate intermediates [22], sulfation of the bimetallic Pd-Pt catalyst possibly changes the reaction route or leads to partial oxidation to some extent. The fact that the intensity of this band decreases with increasing temperature, most likely

22

due to facilitated carbonate desorption and decomposition at higher temperatures, supports this assumption. Moreover, a pronounced band is observed at ~1400 cm^{-1} that can be traced back to surface aluminum sulfates [79-81]. The band with a maximum around 1210 cm^{-1} is assigned to aluminum bulk sulfate species (1208 cm^{-1}, cf. refs. [29, 81]). Since $PdSO_4$ was observed in a similar region (1242 cm^{-1}) [29] and our spectra exhibit broad bands, distinction between these species is difficult. Notably, the data obtained are in good agreement with those reported by Wilburn and Epling [51].
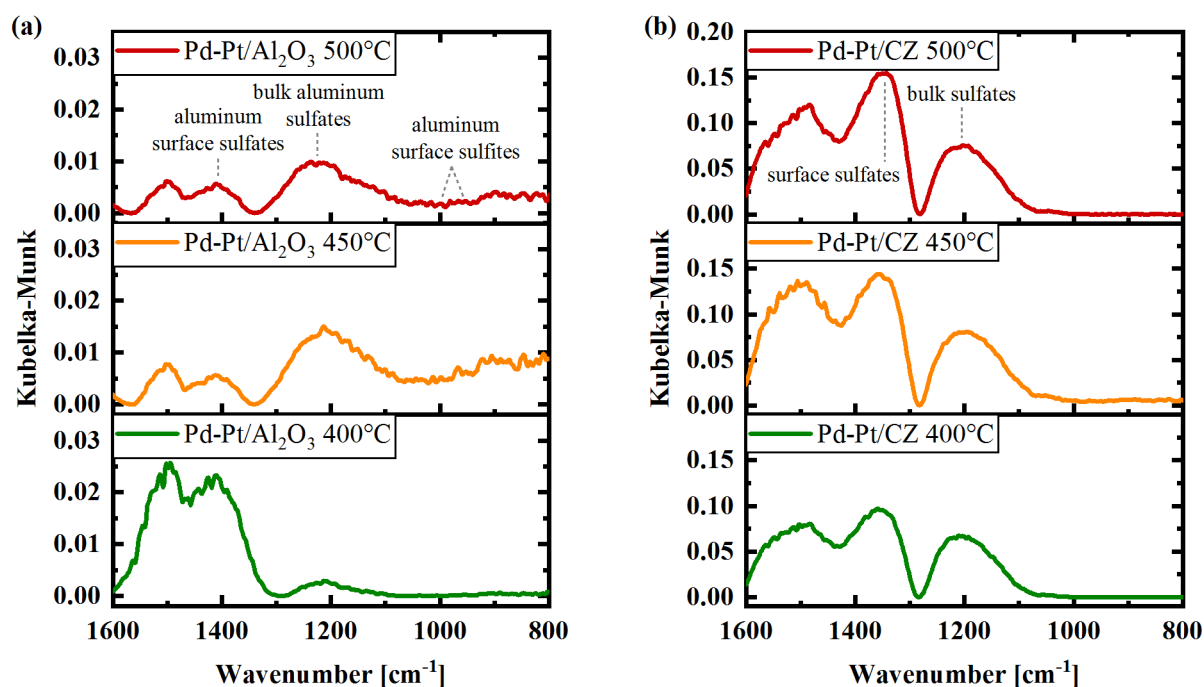
Figure 8. DRIFTS spectra (difference spectra [aged catalyst]-[catalyst as prepared]) obtained for (a) Pd-Pt/Al$_2$O$_3$ and (b) Pt-Pt/CZ after aging the catalyst in 3200 ppm CH$_4$, 10% O$_2$, 12% H$_2$O, 5 ppm SO$_2$ in N$_2$ (GHSV = 80 000 h^{-1}) at 400°C, 450°C or 500°C for 15 h.

The DRIFTS spectra in Figure 8a show that for the Pd-Pt/Al$_2$O$_3$ sample the surface species change significantly with increasing catalyst poisoning temperature. Surface sulfates (bands around 1400 cm^{-1}) decrease, whereas bulk aluminum sulfates (band around 1200 cm^{-1}) form at

elevated temperatures (450°C and 500°C). Considering the activity trends for the alumina supported catalyst samples we can conclude that the increasing bulk sulfation at higher temperatures seems to protect the noble metal to some extent. Hence, this capture of sulfur species results in the remaining catalytic activity observed during the 15 h of aging (Figure 6a). In addition, surface species are obviously less stable at higher temperatures and they are either decomposed or the transfer to the support's bulk is more efficient.

In contrast to the results for the Pd-Pt/Al$_2$O$_3$ catalyst, the DRIFTS spectra for the Pd-Pt/CZ samples in Figure 8b show rather similar band intensities with surface and bulk species after aging at different temperatures. This correlates with the catalytic activity, since the Pd-Pt/CZ catalyst was fully deactivated after aging at all investigated temperatures. For all CZ-based samples, the most pronounced signals are observed at ~1500 and ~1350 cm^{-1}. We attribute the band at ~1500 cm^{-1} to support-related carbonates, which were reported [82] over a Pd/CeO$_2$-ZrO$_2$ catalyst at 1508 cm^{-1} and 1406 cm^{-1}. Köck et al. [83] reported bidentate carbonate signals at 1628, 1431 and 1223 cm^{-1} on zirconia. However, on yttrium-stabilized zirconia they observed slightly shifted signals at 1646, 1429 and 1225 cm^{-1}. The band at ~1350 cm^{-1} could be attributed to surface sulfate species [33, 84-87] on CZ, which could explain the complete loss of activity during the SO$_2$ poisoning experiments. The broad band around 1200 cm^{-1} was assigned to CZ-bulk sulfates. Luo and Gorte [33] reported a broad band for bulk sulfates on a Pd/CeO$_2$ catalyst centered at 1160 cm^{-1}, while exposure of ceria to SO$_2$ and excess O$_2$ leads to bulk sulfation, resulting in a broad band at 1200 cm^{-1} according to Waqif et al. [85].

In summary we can conclude, that an efficient transfer of sulfur species to the support's bulk partially protects the noble metal from activity loss. Our results indicate, that this transfer is more pronounced on alumina, particularly at higher temperatures, whereas the poisoning temperature

does not significantly affect the sulfation process on CZ, resulting in full deactivation for all temperatures investigated.

3.4 Thermal Stability of Sulfur Species

In a next step desorption of sulfur species during heating was conducted after 15 h of sulfur poisoning. The results are shown in Figure 9a. During the S-TPD experiments from Pd-Pt/Al$_2$O$_3$ aged at 400°C, SO$_2$ desorption starts at 540°C, whereas for samples poisoned at higher temperatures, the onset of SO$_2$ desorption is about 50°C higher. This is in agreement with different sulfur species evidenced by DRIFTS (cf. Figure 8). Mainly surface sulfates are formed at low temperatures (400°C), which desorb at lower temperatures, whereas an increase of the aging temperature leads to bulk sulfation. In contrast, the SO$_2$ desorption from Pd-Pt/CZ starts at approximately 480°C, independent from the aging temperature. Moreover, compared to the Al$_2$O$_3$-based catalyst where just one maximum was observed in the SO$_2$-desorption profile due to Al-SO$_x$-compounds, two maxima were recorded for the Pd-Pt/CZ catalyst, at ~610°C and ~760°C (Figure 9a). An additional experiment with a Pd-Pt catalyst supported on pure CeO$_2$ revealed that the first maximum can mostly be attributed to sulfur compounds formed on cerium oxide sites (Figure S8). Literature suggests to attribute the second one to zirconia-linked sulfur species as these are reported to have a higher stability [33, 88]. However, the more stable species could also originate from the special properties of the mixed oxide used in this study. Moreover, the first maximum of the TPD for Pd-Pt/CZ, which we attribute to Ce-SO$_x$-compounds, is less intense for the sample aged at 500°C than for the samples that were aged at lower temperatures. As hardly any changes were visible in DRIFTS, this points to a better quantification by S-TPD.

The total amount of SO$_2$ that is desorbed during the S-TPD as function of aging temperature of the 15 h of sulfur poisoning is shown in Figure 9b. While a significant amount is released after

aging at 400°C, the amount decreases with increasing aging temperature for both catalyst systems. After aging at 400°C, which is typical for the exhaust of lean burn natural gas engines, the released amount of SO_2 is approximately 25% higher for the alumina-based samples compared to Pd-Pt/CZ. Due to its significantly higher surface area alumina should be able to store more (surface) sulfites/sulfates, which might be a possible explanation for the higher SO_2 release. After aging at 450°C and 500°C, on the other hand, more SO_2 was released during the TPD from Pd-Pt/CZ compared to the alumina-based sample.
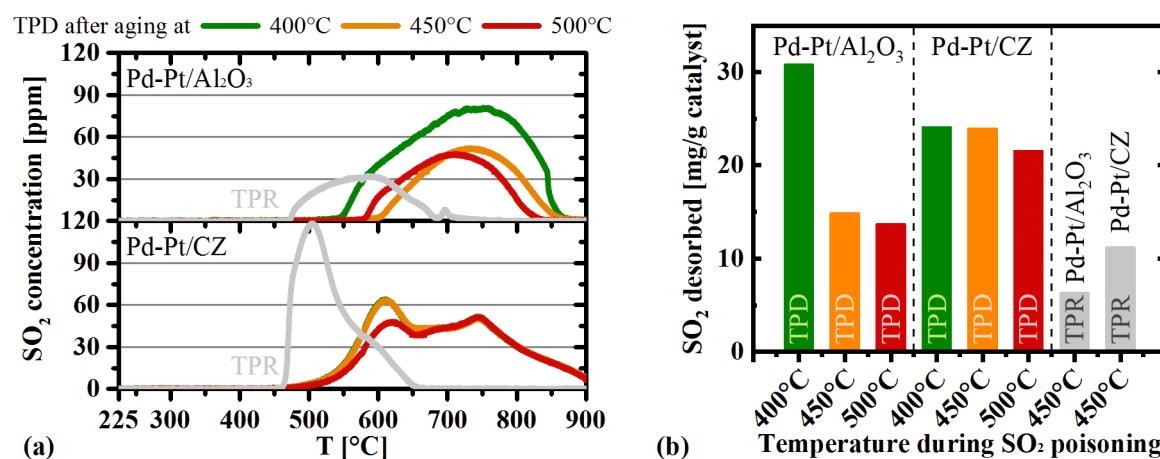
Figure 9. (a) SO_2 desorption profiles and (b) desorbed amount of SO_2 after 15 h of sulfur aging at 450° during TPD in N_2 or CH_4-TPR in 3200 ppm CH_4 in N_2 for Pd-Pt/Al_2O_3 and Pt-Pt/CZ. GHSV = 80 000 h^{-1}. Due to some cross-sensitivity in the FTIR analyzer between CH_4 and SO_2, the values given for desorbed SO_2 amounts during CH_4-TPR are less precise than those for TPD experiments.

To get a complementary insight into the noble metal structure during S-TPD, the catalysts previously poisoned at 450°C at the lab bench were investigated by means of *in situ* XAS during heating to 750°C in He. The full set of data is given in the electronic supporting information (Figures S12a and S12b). The different species occurring (see reference spectra in Figure 3) were quantified by linear combination fitting (LCF) of the XANES data (cf. Figure 10, "TPD").

26

Exemplary fits from LCF analysis of the Pd K-edge XANES spectra during the TPD are shown in Figure S13. According to the results from the LCF analysis, the dominating palladium species in the Pd-Pt/Al$_2$O$_3$ catalyst after poisoning are PdO (~70%) and PdSO$_4$ · 2 H$_2$O (~30%). In good accordance with the TEM/EDXS results this points to predominant surface poisoning of the Pd particles. Analogous, also the evolution of the platinum phase was analyzed by LCF, using reference spectra of PtO$_2$ and metallic Pt (Figure S9). Since Pt exhibits a significantly higher resistance towards SO$_2$ poisoning at this temperature [67] we do not expect Pt-S species in a considerable amount. Platinum is mostly present in oxidized state (PtO$_x$ ~60%), the rest is metallic platinum with some long-range order, which might be due to alloying (Figures S10). Due to the autoreduction of PdO [16], the TPD in pure He results in completely reduced palladium above 600°C (Figure 10). Compared to the decomposition range of 500-550°C reported for PdSO$_4$ · 2 H$_2$O by Dahmen et al. [89], a slight delay is observed in our experiment, with full PdSO$_4$ · 2 H$_2$O reduction only at around 600°C. This stabilization can be explained by the supplementary SO$_x$ evolution from the support material and the significant affinity of PdO to SO$_x$ [67]. Compared to PdO, metallic Pd is less prone to interactions with SO$_x$ [67]. Hence, the autoreduction around 600°C additionally destabilizes Pd-SO$_x$ species and facilitates their full decomposition. Platinum species on the alumina support undergo gradual reduction starting at about 600°C (Figure S10b).

Similar results were obtained for Pd-Pt/CZ, whereby with approximately 40% the initial amount of sulfated species is slightly higher than for the sample supported on alumina (Figure 10), indicating a slightly more pronounced palladium sulfation. Note that the lower signal-to-noise ratio due to the high absorption of X-rays by the CZ support increases the error bars. Hence, detailed information especially on the Pt state were difficult to extract. Nevertheless, a

similar trend like for the alumina-based catalyst was observed during the TPD, with Pt reduction at higher temperature (data not shown). This behavior may be attributed to the high oxygen mobility of CZ, which could be able to keep Pt oxidized up to slightly higher temperatures.
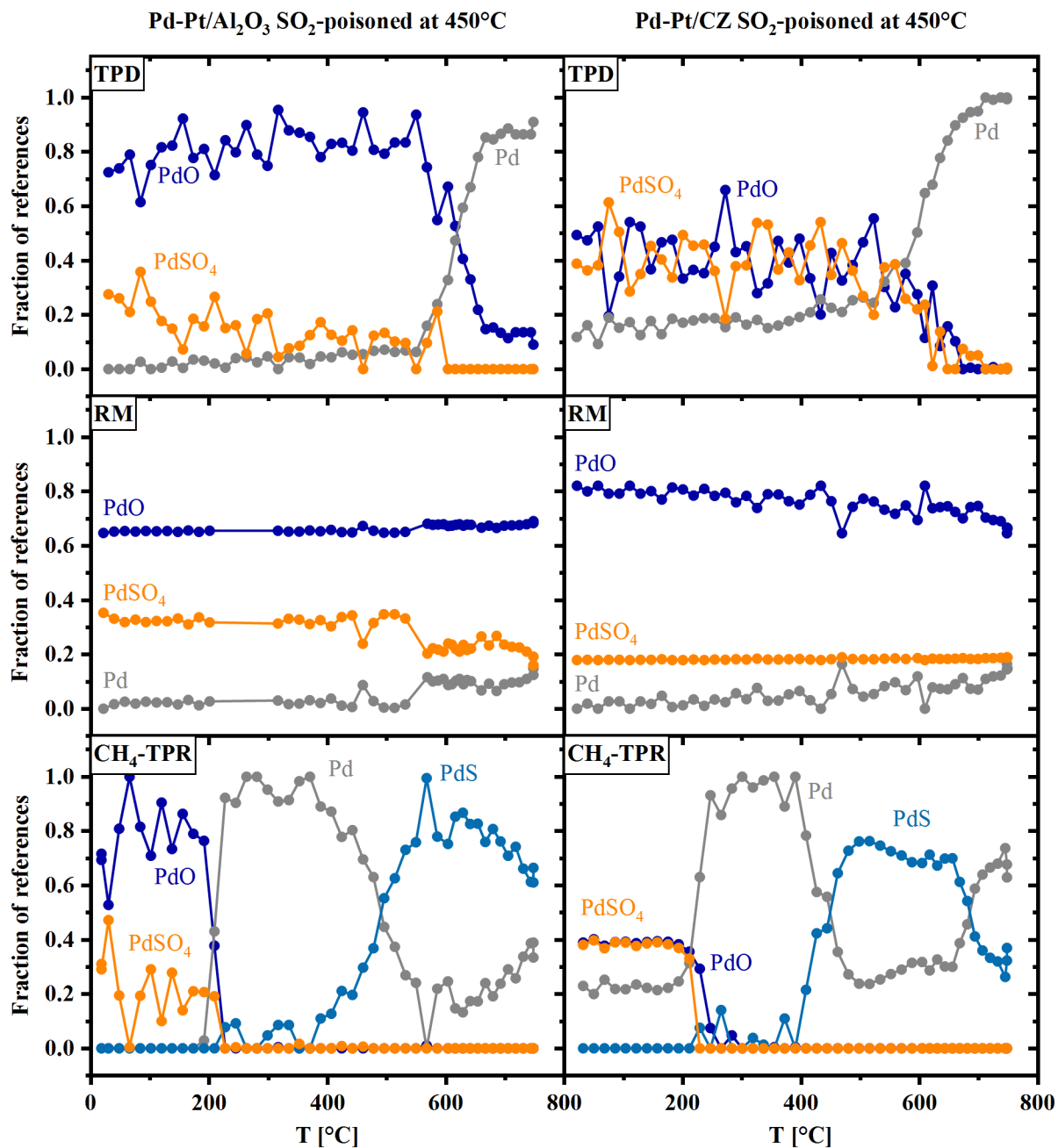
Figure 10. Evolution of Pd-species as fraction of references over temperature for SO_2-poisoned Pd-Pt/Al_2O_3 and Pt-Pt/CZ during heating the samples in GM 1 ("TPD"), GM 2 (reaction mixture, "RM") and GM 3 ("CH_4-TPR") with a ramp rate of 10°C/min.

Complementary to the TPD experiments we additionally investigated the behavior in an oxidative reaction gas mixture containing 3200 ppm CH_4, 10% O_2, 1.5% H_2O in He (GM 2, Table 1). The *in situ* XAS data (Figure 10, "RM"; raw spectra are shown in Figures S12c and S12d, while exemplary fits from LCF analysis are displayed in Figure S14) revealed that irrespective of the support no complete decomposition of the sulfur-poisoned Pd-species could be achieved in the investigated temperature window. At 750°C and under lean conditions the Pd particles in Pd-Pt/Al_2O_3 consisted of ~15% metallic Pd, ~16% $PdSO_4 \cdot 2\ H_2O$ and mainly PdO. Based on thermodynamic calculations (SI) we expected PdO to be the main species under these conditions, with some $PdSO_4$ most probably on the bimetallic particle surface. Our findings that even at such high temperatures the catalyst remains poisoned in an oxidative atmosphere is in line with a study of Wilburn and Epling [52], who reported SO_2 desorption from sulfur poisoned catalysts during temperature programmed oxidation (TPO) but observed only minor recovery, which they attributed to sulfate stabilization by (gas phase) oxygen [54]. Moreover, as SO_2 is desorbed in the presence of O_2 and H_2O, oxidation to SO_3 and H_2SO_4 occurs, maintaining Pd poisoned [27, 30, 67]. The Pd-PdO-$PdSO_4$ phase diagram presented in the supplementary information (Fig. S16) supports these results, as it points to the local partial pressure of SO_x over the noble metal particle as the predominant factor governing $PdSO_4$-stability. A precise quantification of the evolving SO_3 and H_2SO_4 amounts in future experiments, preferably with catalysts that exhibit a varying Pd-Pt ratio, may further clarify the molecular processes on the bimetallic noble metal particles. This could lead to an optimized Pd-Pt ratio with regard to both,

minimized poisoning tendency and maximized bias towards desorption. However, the detection of these low amounts of SO_3 and H_2SO_4 requires an experimental setup with very short and passivated tubing in order to minimize adsorption of the products.

To summarize, thermal decomposition of sulfur species is not an appropriate regeneration concept, neither in inert conditions nor in reaction mixture. Oxidizing conditions keep the active Pd species poisoned due to continuous re-poisoning, hereby preventing sufficient regeneration. The lab-bench TPD experiments in inert conditions revealed, that very high temperatures up to 900°C are necessary to decompose support-related sulfur compounds. In a supplementary decomposition study commercially available bulk sulfates ($Al_2(SO_4)_3$, $Ce(SO_4)_2$, $Zr(SO_4)_2$, $Y_2(SO_4)_3$ and $La_2(SO_4)_3$) were thermally treated in a thermogravimetric analysis device (Figure S17). After releasing the water of crystallization, the order of the onset temperature for decomposition of the sulfur compounds is $Zr(SO_4)_2$ < $Ce(SO_4)_2$ ≤ $Al_2(SO_4)_3$ < $Y_2(SO_4)_3$ < $La_2(SO_4)_3$. The results also indicate, that temperatures above 600°C are necessary to initiate decomposition and thus sulfur release under inert conditions. Full decomposition is only achieved at temperatures typically not reached in lean-burn natural gas engines, such as ~750°C for $Zr(SO_4)_2$, while for the other compounds even higher temperatures are necessary.

3.5 Catalyst Regeneration by Temperature Programmed Reduction (CH₄-TPR)

Previous studies have shown that the regeneration temperature of sulfur poisoned methane oxidation catalysts can significantly be lowered by applying reductive instead of inert or oxidative conditions [44-49, 52]. Hence, the activity tests and 15 h SO_2 poisoning at 450°C were repeated with a fresh sample and followed by a CH₄-TPR in 3200 ppm CH₄ and balance N₂. Desorption experiments showed that the reductive conditions lead to SO_2 desorption at significantly lower temperature compared to inert conditions (grey curves in Figure 9). While the

decomposition of S-species starts at 590°C for Pd-Pt/Al$_2$O$_3$ and around 490°C for Pd-Pt/CZ in nitrogen, the reductive atmosphere leads to SO$_2$ evolution already at 470°C for Pd-Pt/Al$_2$O$_3$ and at 460°C for Pd-Pt/CZ. The SO$_2$ desorption also ends at significantly lower temperatures ($\Delta T \approx$ 100°C for Pd-Pt/Al$_2$O$_3$ and $\Delta T \approx$ 250°C for Pd-Pt/CZ). Obviously rich conditions seem to be a suitable way to remove sulfates/sulfites from sulfur-poisoned catalysts in a reasonable temperature range, particularly, since lean-burn natural gas engines are typically operated in the low temperature regime.

Although using CZ as the support material does not slow down the aging process, sulfur desorption seems to be facilitated under the chosen conditions. As shown in Figure 9b, larger amounts of SO$_2$ are desorbed during TPD and CH$_4$-TPR from Pd-Pt/CZ – at least without taking possible H$_2$S formation into account, which is discussed below. Moreover, SO$_2$ desorption starts and ends at lower temperatures compared to Pd-Pt/Al$_2$O$_3$. This is in line with results of Waqif et al. [86] who reported an easier reducibility of sulfates on CeO$_2$-containing materials in comparison to alumina when treating the samples with H$_2$. Our supplementary decomposition study on bulk sulfates supports these findings, as significant decomposition of Ce(SO$_4$)$_2$ is initiated at about 650°C in 5% CH$_4$ and balance He, while Al$_2$(SO$_4$)$_3$ decomposition starts approximately 50°C later (Figure S17). With respect to the possible catalyst regeneration procedures, Pd-Pt/CZ also shows significantly less spillover of remaining sulfur species to the noble metal than the alumina-based catalyst. We could show this behavior in one of our previous studies [49] and observed full recovery of the catalytic activity for Pd-Pt/CZ, whereas Pd-Pt/Al$_2$O$_3$ only partially regained its activity.

When comparing the total amounts of desorbed SO$_2$ from the two poisoned catalysts at 450°C during the TPD and CH$_4$-TPR measurements (Figure 9b and Figures S18 and S19), less SO$_2$ is

detected during the CH_4-TPR. This behavior can be explained by formation of other sulfur compounds in the presence of CH_4, e.g. COS or H_2S (cf. Figure S19), which are subsequently desorbed or re-adsorbed on the catalyst, or by transformation of sulfur compounds that remain on the support [32, 33, 50].

To understand the impact of the rich conditions on the noble metal state, the same TPR experiment in 3200 ppm CH_4 in He (GM 3, Table 1) was performed while monitoring the Pd K-edge and the Pt L_3-edge by *in situ* XANES. The initial 60% of PtO_2 of the Pd-Pt/Al_2O_3 catalyst are reduced at approximately 300°C during the TPR, finally resulting in fully reduced platinum (Figure S11). A similar trend was observed for Pt L_3-edge measurements of Pd-Pt/CZ (data not shown, too low signal-to-noise ratio). Interestingly, LCF analysis of the obtained Pd K-edge XANES spectra with reference spectra reveals three different regimes for the Pd-species (Figure 10, "TPR"). Both catalysts remain in their initial poisoned state in the low-temperature regime. At around 200°C a transformation to metallic Pd occurs. Further heating leads to significant conversion from Pd to PdS, which starts to form at approximately 400°C. While the maximum PdS amount of ~85% is observed at around 600°C for Pd-Pt/Al_2O_3, the maximum PdS content is approximately 75% at about 500°C on the CZ-supported sample. The transformation of PdS induced by higher temperatures is less pronounced for the alumina-based sample, ending with an approximate PdS:Pd ratio of 60:40 at 750°C, whereas at the same temperature it is 35:65 for Pd-Pt/CZ.

PdS may form via two pathways:

(i) Reaction of metallic Pd with H_2S, which is formed by reduction on the catalyst surface of the SO_2 evolved during $PdSO_4$ decomposition in the presence of CH_4. H_2S is known to form Pd-S compounds with palladium [90], in particular Pd_4S. The hypothesis is supported by results

of Nissinen et al. [55] who observed Pd_4S by means of powder XRD when exposing $PdSO_4$ to 10% H_2 in Ar. Performing a TPR of a SO_2 poisoned Pd-Pt/Al_2O_3 sample in a CH_4-containing gas mixture using a thermal gravimetric analysis device equipped with a mass spectrometer reveals that besides SO_2 also H_2S, COS and CS_2 can be detected (Figure S19a). Obviously, the latter species form during the experiment and can interact with the palladium species. Although no significant amounts of H_2S were monitored during the TPR treatment of the Pd-Pt/CZ catalyst, the trend of the CH_4 signal also suggests H_2S formation (Figure S19b). Probably the low amount of sample used in the TGA setup released so few H_2S that it was below the detection limit of the mass spectrometer. Moreover, we can also speculate about H_2S formation on the catalyst's surface, which immediately reacts with metallic Pd and forms PdS without desorption, or we could think about a second decomposition mechanism.

(ii) PdS formation via direct reduction of $PdSO_4$ to PdS:

$$PdSO_4 \ + \ CH_4 \ \rightarrow \ PdS \ + \ 2 \, H_2O \ + \ CO_2.$$

Already in 1993, Hoyos et al. [91] suggested a similar mechanism in the presence of hydrogen ($PdSO_4 + 4 \, H_2 \rightarrow PdS + 4 \, H_2O$), however, without presenting clear evidence for this theory.

Due to the presence of water under realistic conditions, the TPR was also performed in a water containing gas mixture (3200 ppm CH_4, 1.5% H_2O, balance He/N_2, GM 4, Table 1) at both, the beamline and the lab-bench. Compared to the water-free TPR no major differences were observed during the *in situ* XAS experiment. The initial mixture of mainly PdO and $PdSO_4 \cdot 2$ H_2O experiences sudden reduction to metallic Pd at around 200°C, which is subsequently transformed into PdS at elevated temperatures (Figure S15). A minor delay in reduction can be surmised, which might point to a slight stabilization of $PdSO_4 \cdot 2 \, H_2O$ in the presence of water. However, the amount of PdS that forms during the TPR seems to be slightly lower compared to

the H_2O-free conditions. The maximum PdS concentration is approximately 50% on Pd-Pt/Al_2O_3, whereas only 40% were observed for Pd-Pt/CZ. Rich regeneration in dry conditions, on the other hand, leads to quasi-exclusive presence of PdS on alumina and at least 80% PdS on the CZ support in a similar temperature range (Figure 10).

In one of our previous studies [56] we found PdS being unstable in the presence of oxygen and observed immediate transformation to PdO. Complementary activity tests after regenerating a sulfur poisoned sample of each catalyst formulation by application of a TPR up to 750°C confirm these findings. The comparison between the activity in the fresh, poisoned and regenerated state reveals, that full regeneration in 3200 ppm CH_4 and balance N_2 is only possible for Pd-Pt/CZ (Figure 11). Although also Pd-Pt/Al_2O_3 regains catalytic activity by the reductive high-temperature treatment, the TPR in dry rich conditions does not fully recover the catalytic activity. In contrast, full regeneration was possible if water was present during the rich treatment. Notably, except for the light-off of Pd-Pt/Al_2O_3 after regeneration by a dry TPR, the light-off curves are even shifted towards lower temperatures after the reductive regeneration. This supports our recent study, in which we report a temporary activity increase of palladium-based methane oxidation catalysts after prereduction prior to a light-off test [23].
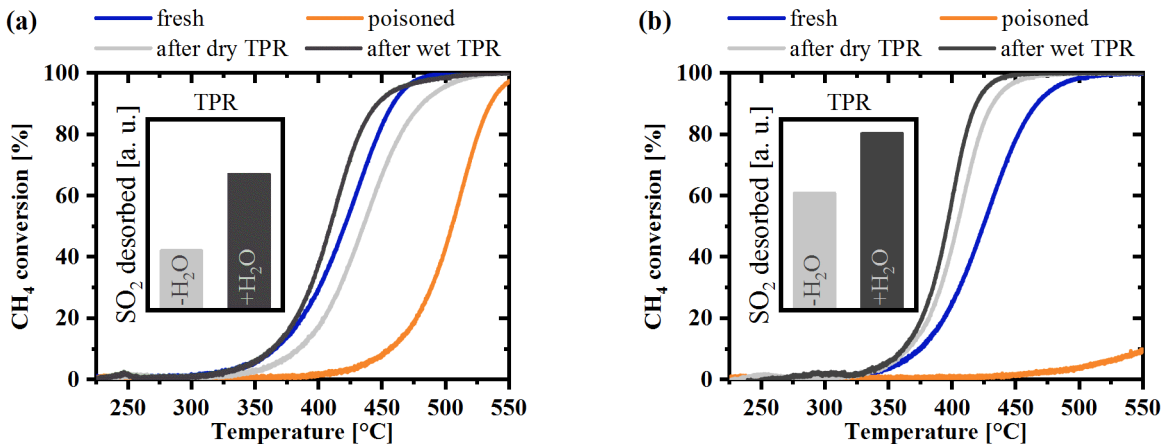
Figure 11. Light-off curves for (a) Pd-Pt/Al₂O₃ and (b) Pd-Pt/CZ in the fresh, poisoned and regenerated state after performing a TPR up to 750°C in 3200 ppm CH_4 in N_2 (dry CH_4-TPR, -H_2O) or 3200 ppm CH_4, 12% H_2O in N_2 (wet CH_4-TPR, +H_2O). GHSV = 80 000 h^{-1}.

Despite the very similar results during dry and wet CH_4-TPR regeneration when following the noble metal state with *in situ* XAS, the presence of H_2O during the rich treatment obviously plays an important role. We found less SO_2 desorption occurring during the dry CH_4-TPR, while significantly more SO_2 was desorbed in the presence of steam, which resulted in complete regeneration (Figure 11). Luo et al. [92] reported similar results for a Pt/Al₂O₃ model catalyst and found, that the temperature of the sulfur desorption onset is lower when H_2O is added to the reductive reaction environment. It was speculated, that water reacts with the support-related sulfates of the form $(Al_3O_3)S = O$, resulting in formation of $(Al_2O_2)SO(OH)$ [93], which lowers the desorption energy. Moreover, steam reforming of CH_4 with H_2O may occur on the noble metal particles, resulting in H_2 formation. The reaction of this H_2 with sulfur compounds to H_2S could further facilitate the removal of sulfur from the catalyst, hereby benefiting the regeneration. In this context, further fundamental investigations concerning the underlying mechanism are highly desirable in the future.

Equally important, the probability for re-poisoning by spillover of remaining sulfur compounds to palladium decreases with increasing amounts of desorbed SO_x, which plays a particular role on alumina supported catalysts. For instance, Honkanen et al. [50] report that remaining $Al_2(SO_4)_3$ has an even stronger effect on the catalyst performance than the oxidation state of Pd/PdO as spillover of sulfur species to the noble metal leads to re-poisoning. These findings are further supported by Kinnunen et al. [94], who claim that the presence of aluminum sulfate hinders palladium reoxidation after a reductive regeneration treatment. In this regard usage of CZ as support material seems to be the better choice compared to alumina. We did not only observe less spillover in one of our previous studies [49], but also found in the present study that under rich conditions SO_2 desorption and full sulfur species decomposition occur at lower temperatures. Hence, further optimization of catalyst properties, e.g. by rationally designing novel materials, is highly desirable in future studies.

4. Conclusions

SO_2 poisoning and different catalyst regeneration strategies were investigated for Pd-Pt/Al_2O_3 and Pd-Pt/CeO_2-ZrO_2-Y_2O_3-La_2O_3 catalysts by combining comprehensive lab-bench catalyst tests and characterization of the sulfur aged samples by TEM, DRIFTS, XRD and *ex situ/ in situ* XAS measurements at the S K-, Pd K- and Pt L_3-edges. The systematic studies of the aging revealed, that sulfating supports such as Al_2O_3 remain indispensable, as these are able to protect the noble metal at least to some extent by formation of sulfur compounds. While Pd-Pt/Al_2O_3 retains limited activity after the sulfur poisoning, Pd-Pt/CeO_2-ZrO_2-Y_2O_3-La_2O_3 is fully deactivated, emphasizing the tremendous importance of the support. We attribute this difference to more efficient transfer of surface sulfates to the bulk of alumina at elevated temperatures,

while irrespective of the aging temperature the noble metal is stronger affected on CeO$_2$-ZrO$_2$-Y$_2$O$_3$-La$_2$O$_3$. Compared to desorption of sulfur species under inert or lean conditions, only rich conditions lead to a pronounced reactivation. In addition, regeneration of sulfur poisoned catalysts was systematically investigated by *in situ* XAS combined with CH$_4$-TPR experiments, unraveling three different states of the catalyst during the regeneration process under the most efficient rich conditions. While the catalyst remains poisoned below 200°C, decomposition of PdSO$_4$ that formed during sulfur aging occurs above this temperature under rich conditions, leading to formation of metallic Pd. However, further increase in temperature, which is necessary for regeneration of the support material, results in re-poisoning of the noble metal, as PdS formation was observed. Moreover, it was found that the presence of water during the catalyst regeneration in a reductive atmosphere, i.e. CH$_4$ rich, highly facilitates the desorption of support-related SO$_2$ and results in complete recovery of the catalytic activity. These structural transformations, the critical nature of the support and the role of the reaction atmosphere need to be taken into account when developing regeneration strategies for long-term application of methane oxidation catalysts, since residual sulfides on the noble metal but also on the support material lead to sulfate formation (PdSO$_x$) [91] and can hereby contribute to long-term poisoning. To ensure high catalytic activity, it is crucial to either avoid PdS formation during the regeneration process, or to fully decompose the formed PdS as well as all sulfur species stored on the support before the methane oxidation reaction starts again.

While further investigations might complement the fundamental mechanistic understanding during sulfur poisoning and consecutive regeneration, the applied *in situ* methods shined detailed light on the role of the support material and of the noble metal of bimetallic palladium-platinum methane oxidation catalysts under conditions relevant for practical applications. Such a

comprehensive knowledge is crucial for deducing optimal regeneration conditions for sulfur poisoned catalysts, since this is a key step for the establishment of an industry-relevant long-term operation of methane oxidation catalysts and the economically and ecologically sustainable application of natural gas engines.

ASSOCIATED CONTENT

Supporting Information. Additional information on catalyst characterization, catalyst testing and evolution of species during XAS investigations as derived from LCF, as well as supplementary decomposition experiments (PDF).

AUTHOR INFORMATION

Corresponding Author

*Olaf Deutschmann, Institute for Chemical Technology and Polymer Chemistry (ITCP), Karlsruhe Institute of Technology (KIT), Kaiserstr. 12, 76131 Karlsruhe, Germany, Tel.: +49 721 608 43064, Fax: +49 721 608 44805, deutschmann@kit.edu

*Jan-Dierk Grunwaldt, Institute for Chemical Technology and Polymer Chemistry (ITCP), Karlsruhe Institute of Technology (KIT), Kaiserstr. 12, 76131 Karlsruhe, Germany, Tel.: +49 721 608 42120, Fax: +49 721 608 44820, grunwaldt@kit.edu

Author Contributions

The manuscript was written through contributions of all authors. All authors have given approval to the final version of the manuscript.

Funding Sources

Notes

The authors declare not competing financial interest.

ABBREVIATIONS

BET, Brunauer-Emmet-Teller; BF, bright field; CEM, controlled evaporator and mixer; CZ, CeO_2-ZrO_2-Y_2O_3-La_2O_3; DCM, double crystal monochromator; DRIFTS, diffuse reflectance Fourier-transform infrared spectroscopy; EDXS, energy-dispersive X-ray spectroscopy; EXAFS, extended X-ray absorption fine structure; FTIR, Fourier-transform infrared spectroscopy; GM, gas mixture; HAADF, high-angle annular dark field ; ICP-OES, inductively coupled plasma optical emission spectrometry; i.d., inner diameter; LCF, linear combination fitting; MFC, mass flow controller; (S)TEM, (s)canning transmission electron microscopy; TPD, temperature programmed desorption; TPO, temperature programmed oxidation; TPR, temperature programmed reduction; XANES, X-ray absorption near-edge structure; XAS, X-ray absorption spectroscopy; XRD, X-ray diffraction.

REFERENCES

[1] R.W. Howarth, A bridge to nowhere: methane emissions and the greenhouse gas footprint of natural gas, Energy Sci. Eng., 2 (2014) 47-60.

[2] Y.F.Y. Yao, Oxidation of Alkanes over Noble-Metal Catalysts, Ind. Eng. Chem. Prod. Res. Dev., 19 (1980) 293-298.

[3] O. Deutschmann, J.-D. Grunwaldt, Exhaust Gas Aftertreatment in Mobile Systems: Status, Challenges, and Perspectives, Chem. Ing. Tech., 85 (2013) 595-617.

[4] P. Gelin, M. Primet, Complete oxidation of methane at low temperature over noble metal based catalysts: a review, Appl. Catal. B, 39 (2002) 1-37.

[5] D. Ciuparu, M.R. Lyubovsky, E. Altman, L.D. Pfefferle, A. Datye, Catalytic combustion of methane over palladium-based catalysts, Catal. Rev.: Sci. Eng., 44 (2002) 593-649.

[6] R. Burch, F.J. Urbano, P.K. Loader, Methane Combustion over Palladium Catalysts - the Effect of Carbon-Dioxide and Water on Activity, Appl. Catal. A, 123 (1995) 173-184.

[7] R. Kikuchi, S. Maeda, K. Sasaki, S. Wennerstrom, K. Eguchi, Low-temperature methane oxidation over oxide-supported Pd catalysts: inhibitory effect of water vapor, Appl. Catal. A, 232 (2002) 23-28.

[8] R. Gholami, M. Alyani, K.J. Smith, Deactivation of Pd Catalysts by Water during Low Temperature Methane Oxidation Relevant to Natural Gas Vehicle Converters, Catalysts, 5 (2015) 561-594.

[9] M. Alyani, K.J. Smith, Kinetic Analysis of the Inhibition of CH_4 Oxidation by H_2O on PdO/Al_2O_3 and $CeO_2/PdO/Al_2O_3$ Catalysts, Ind. Eng. Chem. Res., 55 (2016) 8309-8318.

[10] K. Narui, H. Yata, K. Furuta, A. Nishida, Y. Kohtoku, T. Matsuzaki, Effects of addition of Pt to PdO/Al_2O_3 catalyst on catalytic activity for methane combustion and TEM observations of supported particles, Appl. Catal. A, 179 (1999) 165-173.

[11] G. Lapisardi, L. Urfels, P. Gelin, M. Primet, A. Kaddouri, E. Garbowski, S. Toppi, E. Tena, Superior catalytic behaviour of Pt-doped Pd catalysts in the complete oxidation of methane at low temperature, Catal. Today, 117 (2006) 564-568.

[12] P. Castellazzi, G. Groppi, P. Forzatti, Effect of Pt/Pd ratio on catalytic activity and redox behavior of bimetallic $Pt-Pd/Al_2O_3$ catalysts for CH_4 combustion, Appl. Catal. B, 95 (2010) 303-311.

[13] K. Persson, A. Ersson, K. Jansson, J.L.G. Fierro, S.G. Jaras, Influence of molar ratio on Pd-Pt catalysts for methane combustion, J. Catal., 243 (2006) 14-24.

[14] R. Burch, F.J. Urbano, Investigation of the Active State of Supported Palladium Catalysts in the Combustion of Methane, Appl. Catal. A, 124 (1995) 121-138.

[15] A.K. Datye, J. Bravo, T.R. Nelson, P. Atanasova, M. Lyubovsky, L. Pfefferle, Catalyst microstructure and methane oxidation reactivity during the Pd <–> PdO transformation on alumina supports, Appl. Catal. A, 198 (2000) 179-196.

[16] J.-D. Grunwaldt, N. van Vegten, A. Baiker, Insight into the structure of supported palladium catalysts during the total oxidation of methane, Chem. Commun., (2007) 4635-4637.

[17] S.K. Matam, M.H. Aguirre, A. Weidenkaff, D. Ferri, Revisiting the Problem of Active Sites for Methane Combustion on Pd/Al_2O_3 by Operando XANES in a Lab-Scale Fixed-Bed Reactor, J. Phys. Chem. C, 114 (2010) 9439-9443.

[18] A. Hellman, A. Resta, N.M. Martin, J. Gustafson, A. Trinchero, P.A. Carlsson, O. Balmes, R. Felici, R. van Rijn, J.W.M. Frenken, J.N. Andersen, E. Lundgren, H. Grönbeck, The Active Phase of Palladium during Methane Oxidation, J. Phys. Chem. Lett., 3 (2012) 678-682.

[19] G.S. Bugosh, V.G. Easterling, I.A. Rusakova, M.P. Harold, Anomalous steady-state and spatio-temporal features of methane oxidation on $Pt/Pd/Al_2O_3$ monolith spanning lean and rich conditions, Appl. Catal. B, 165 (2015) 68-78.

[20] H. Nassiri, K.E. Lee, Y.F. Hu, R.E. Hayes, R.W.J. Scott, N. Semagina, Water shifts PdO-catalyzed lean methane combustion to Pt-catalyzed rich combustion in Pd-Pt catalysts: In situ X-ray absorption spectroscopy, J. Catal., 352 (2017) 649-656.

[21] Y. Mahara, K. Murata, K. Ueda, J. Ohyama, K. Kato, A. Satsuma, Time Resolved in situ DXAFS Revealing Highly Active Species of PdO Nanoparticle Catalyst for CH_4 Oxidation, ChemCatChem, 10 (2018) 3384-3387.

[22] H. Stotz, L. Maier, A. Boubnov, A.T. Gremminger, J.-D. Grunwaldt, O. Deutschmann, Surface reaction kinetics of methane oxidation over PdO, J. Catal., 370 (2019) 152-175.

[23] P. Lott, P. Dolcet, M. Casapu, J.-D. Grunwaldt, O. Deutschmann, The Effect of Prereduction on the Performance of Pd/Al$_2$O$_3$ and Pd/CeO$_2$ Catalysts during Methane Oxidation, Ind. Eng. Chem. Res., 58 (2019) 12561-12570.

[24] D. Ciuparu, F. Bozon-Verduraz, L. Pfefferle, Oxygen exchange between palladium and oxide supports in combustion catalysts, J. Phys. Chem. B, 106 (2002) 3434-3442.

[25] D. Ciuparu, L. Pfefferle, Contributions of lattice oxygen to the overall oxygen balance during methane combustion over PdO-based catalysts, Catal. Today, 77 (2002) 167-179.

[26] P. Gelin, L. Urfels, M. Primet, E. Tena, Complete oxidation of methane at low temperature over Pt and Pd catalysts for the abatement of lean-burn natural gas fuelled vehicles emissions: influence of water and sulphur containing compounds, Catal. Today, 83 (2003) 45-57.

[27] T. Hamzehlouyan, C. Sampara, J.N. Li, A. Kumar, W. Epling, Sulfur Poisoning of a Pt/Al$_2$O$_3$ Oxidation Catalyst: Understanding of SO$_2$, SO$_3$ and H$_2$SO$_4$ Impacts, Top. Catal., 59 (2016) 1028-1032.

[28] D.L. Mowery, M.S. Graboski, T.R. Ohno, R.L. McCormick, Deactivation of PdO-Al$_2$O$_3$ oxidation catalyst in lean-burn natural gas engine exhaust: aged catalyst characterization and studies of poisoning by H$_2$O and SO$_2$, Appl. Catal. B, 21 (1999) 157-169.

[29] D.L. Mowery, R.L. McCormick, Deactivation of alumina supported and unsupported PdO methane oxidation catalyst: the effect of water on sulfate poisoning, Appl. Catal. B, 34 (2001) 287-297.

[30] M. Monai, T. Montini, M. Melchionna, T. Duchon, P. Kus, C. Chen, N. Tsud, L. Nasi, K.C. Prince, K. Veltruska, V. Matolin, M.M. Khader, R.J. Gorte, P. Fornasiero, The effect of sulfur dioxide on the activity of hierarchical Pd-based catalysts in methane combustion, Appl. Catal. B, 202 (2017) 72-83.

[31] T.C. Yu, H. Shaw, The effect of sulfur poisoning on methane oxidation over palladium supported on γ-alumina catalysts, Appl. Catal. B, 18 (1998) 105-114.

[32] T. Luo, J.M. Vohs, R.J. Gorte, An Examination of Sulfur Poisoning on Pd/Ceria Catalysts, J. Catal., 210 (2002) 397-404.

[33] T. Luo, R.J. Gorte, Characterization of SO_2-poisoned ceria-zirconia mixed oxides, Appl. Catal. B, 53 (2004) 77-85.

[34] O. Kröcher, M. Widmer, M. Elsener, D. Rothe, Adsorption and Desorption of SOx on Diesel Oxidation Catalysts, Ind. Eng. Chem. Res., 48 (2009) 9847-9857.

[35] M.Y. Smirnov, A.V. Kalinkin, A.V. Pashis, I.P. Prosvirin, V.I. Bukhtiyarov, Interaction of SO_2 with Pt Model Supported Catalysts Studied by XPS, J. Phys. Chem. C, 118 (2014) 22120-22135.

[36] T. Hamzehlouyan, C.S. Sampara, J.H. Li, A. Kumar, W.S. Epling, Kinetic study of adsorption and desorption of SO_2 over γ-Al_2O_3 and Pt/γ-Al_2O_3, Appl. Catal. B, 181 (2016) 587-598.

[37] N. Sadokhina, G. Smedler, U. Nylen, M. Olofsson, L. Olsson, Deceleration of SO_2 poisoning on PtPd/Al_2O_3 catalyst during complete methane oxidation, Appl. Catal. B, 236 (2018) 384-395.

[38] J.K. Lampert, M.S. Kazi, R.J. Farrauto, Palladium catalyst performance for methane emissions abatement from lean burn natural gas vehicles, Appl. Catal. B, 14 (1997) 211-223.

[39] D.E. Doronkin, T.S. Khan, T. Bligaard, S. Fogel, P. Gabrielsson, S. Dahl, Sulfur poisoning and regeneration of the Ag/γ-Al_2O_3 catalyst for H_2-assisted SCR of NOx by ammonia, Appl. Catal. B, 117 (2012) 49-58.

[40] S. Matsumoto, Y. Ikeda, H. Suzuki, M. Ogai, N. Miyoshi, NOx storage reduction catalyst for automotive exhaust with improved tolerance against sulfur poisoning, Appl. Catal. B, 25 (2000) 115-124.

[41] H. Hirata, I. Hachisuka, Y. Ikeda, S. Tsuji, S. Matsumoto, NOx storage-reduction three-way catalyst with improved sulfur tolerance, Top. Catal., 16 (2001) 145-149.

[42] T. Schedlbauer, P. Lott, M. Casapu, H. Stormer, O. Deutschmann, J.-D. Grunwaldt, Impact of the Support on the Catalytic Performance, Inhibition Effects and SO_2 Poisoning Resistance of Pt-Based Formaldehyde Oxidation Catalysts, Top. Catal., 62 (2019) 198-205.

[43] D.E. Doronkin, S. Fogel, P. Gabrielsson, J.-D. Grunwaldt, S. Dahl, Ti and Si doping as a way to increase low temperature activity of sulfated Ag/Al_2O_3 in H_2-assisted NH_3-SCR of NOx, Appl. Catal. B, 148 (2014) 62-69.

[44] J.K. Lampert, M.S. Kazi, R.J. Farrauto, Methane Emissions Abatement from Lean Burn Natural Gas Vehicle Exhaust: Sulfur's Impact on Catalyst Performance, SAE Technical Paper 961971, (1996).

[45] J.M. Jones, V.A. Dupont, R. Brydson, D.J. Fullerton, N.S. Nasri, A.B. Ross, A.V.K. Westwood, Sulphur poisoning and regeneration of precious metal catalysed methane combustion, Catal. Today, 81 (2003) 589-601.

[46] S. Ordonez, P. Hurtado, F.V. Diez, Methane catalytic combustion over Pd/Al_2O_3 in presence of sulphur dioxide: development of a regeneration procedure, Catal. Lett., 100 (2005) 27-34.

[47] F. Arosio, S. Colussi, G. Groppi, A. Trovarelli, Regeneration of S-poisoned Pd/Al_2O_3 catalysts for the combustion of methane, Catal. Today, 117 (2006) 569-576.

[48] F. Arosio, S. Colussi, A. Trovarelli, G. Groppi, Effect of alternate CH_4-reducing/lean combustion treatments on the reactivity of fresh and S-poisoned $Pd/CeO_2/Al_2O_3$ catalysts, Appl. Catal. B, 80 (2008) 335-342.

[49] A. Gremminger, P. Lott, M. Merts, M. Casapu, J.-D. Grunwaldt, O. Deutschmann, Sulfur poisoning and regeneration of bimetallic Pd-Pt methane oxidation catalysts, Appl. Catal. B, 218 (2017) 833-843.

[50] M. Honkanen, J. Wang, M. Kärkkäinen, M. Huuhtanen, H. Jiang, K. Kallinen, R.L. Keiski, J. Akola, V. Minnamari, Regeneration of sulfur-poisoned Pd-based catalyst for natural gas oxidation, J. Catal., 358 (2018) 253-256.

[51] M.S. Wilburn, W.S. Epling, SO_2 adsorption and desorption characteristics of Pd and Pt catalysts: Precious metal crystallite size dependence, Appl. Catal. A, 534 (2017) 85-93.

[52] M.S. Wilburn, W.S. Epling, Sulfur deactivation and regeneration of mono- and bimetallic Pd-Pt methane oxidation catalysts, Appl. Catal. B, 206 (2017) 589-598.

[53] M.S. Wilburn, W.S. Epling, SO_2 adsorption and desorption characteristics of bimetallic Pd-Pt catalysts: Pd: Pt ratio dependency, Catal. Today, 320 (2019) 11-19.

[54] M.S. Wilburn, W.S. Epling, Formation and Decomposition of Sulfite and Sulfate Species on Pt/Pd Catalysts: An SO_2 Oxidation and Sulfur Exposure Study, ACS Catal., 9 (2019) 640-648.

[55] V.H. Nissinen, N.M. Kinnunen, M. Suvanto, Regeneration of a sulfur-poisoned methane combustion catalyst: Structural evidence of Pd_4S formation, Appl. Catal. B, 237 (2018) 110-115.

[56] P. Lott, M. Eck, D.E. Doronkin, R. Popescu, M. Casapu, J.-D. Grunwaldt, O. Deutschmann, Regeneration of Sulfur Poisoned $Pd-Pt/CeO_2-ZrO_2-Y_2O_3-La_2O_3$ and $Pd-Pt/Al_2O_3$ Methane Oxidation Catalysts, Top. Catal., 62 (2019) 164-171.

[57] W. Kleist, J.-D. Grunwaldt, High Output Catalyst Development in Heterogeneous Gas Phase Catalysis, in: A. Hagemeyer, A.F. Volpe (Eds.) Modern Applications of High Throughput R&D in Heterogeneous Catalysis, Bentham Science Publishers 2014, pp. 357-371.

[58] A.M. Gänzler, M. Casapu, P. Vernoux, S. Loridant, F.J.C.S. Aires, T. Epicier, B. Betz, R. Hoyer, J.-D. Grunwaldt, Tuning the Structure of Platinum Particles on Ceria In Situ for Enhancing the Catalytic Performance of Exhaust Gas Catalysts, Angew. Chem., Int. Ed., 56 (2017) 13078-13082.

[59] S. Brunauer, P.H. Emmett, E. Teller, Adsorption of gases in multimolecular layers, J. Am. Chem. Soc., 60 (1938) 309-319.

[60] A. Zimina, K. Dardenne, M.A. Denecke, D.E. Doronkin, E. Huttel, H. Lichtenberg, S. Mangold, T. Prüßmann, J. Rothe, T. Spangenberg, R. Steininger, T. Vitova, H. Geckeis, J.-D. Grunwaldt, CAT-ACT – A new highly versatile x-ray spectroscopy beamline for catalysis and radionuclide science at the KIT synchrotron light facility ANKA, Rev. Sci. Instrum., 88 (2017) 113113.

[61] T. Spangenberg, J. Göttlicher, R. Steininger, An Efficient Referencing And Sample Positioning System To Investigate Heterogeneous Substances With Combined Microfocused Synchrotron X-ray Techniques, AIP Conf. Proc., 1092 (2009) 93-97.

[62] V. Briois, C. La Fontaine, S. Belin, L. Barthe, T. Moreno, V. Pinty, A. Carcy, R. Girardot, E. Fonda, ROCK: the new Quick-EXAFS beamline at SOLEIL, J. Phys.: Conf. Ser., 712 (2016) 012149.

[63] C. La Fontaine, L. Barthe, A. Rochet, V. Briois, X-ray absorption spectroscopy and heterogeneous catalysis: Performances at the SOLEIL's SAMBA beamline, Catal. Today, 205 (2013) 148-158.

[64] W.A. Caliebe, V. Murzin, A. Kalinko, M. Görlitz, High-flux XAFS-beamline P64 at PETRA III, AIP Conf. Proc., 2054 (2019) 060031.

[65] B. Ravel, M. Newville, ATHENA, ARTEMIS, HEPHAESTUS: data analysis for X-ray absorption spectroscopy using IFEFFIT, J. Synchrotron Radiat., 12 (2005) 537-541.

[66] D. Bazin, J.J. Rehr, Comment on "Operando DRIFTS and XANES Study of Deactivating Effect of CO_2 on a $Ce_{0.8}Cu_{0.2}O_2$ CO-PROX Catalyst", J. Phys. Chem. C, 115 (2011) 23233-23236.

[67] H.N. Sharma, V. Sharma, A.B. Mhadeshwar, R. Ramprasad, Why Pt Survives but Pd Suffers From SOx Poisoning?, J. Phys. Chem. Lett., 6 (2015) 1140-1148.

[68] A.F. Hollemann, E. Wiberg, N. Wiberg, Lehrbuch der Anorganischen Chemie, de Gruyter, Berlin, 2007.

[69] J. Jones, H.F. Xiong, A.T. Delariva, E.J. Peterson, H. Pham, S.R. Challa, G.S. Qi, S. Oh, M.H. Wiebenga, X.I.P. Hernandez, Y. Wang, A.K. Datye, Thermally stable single-atom platinum-on-ceria catalysts via atom trapping, Science, 353 (2016) 150-154.

[70] D. Li, G.M. Bancroft, M. Kasrai, M.E. Fleet, X.H. Feng, K. Tan, S-K-Edge and L-Edge X-Ray-Absorption Spectroscopy of Metal Sulfides and Sulfates - Applications in Mineralogy and Geochemistry, Can. Mineral., 33 (1995) 949-960.

[71] R. Sarangi, P. Frank, K.O. Hodgson, B. Hedman, When identical functional groups are not identical: A DFT study of the effects of molecular environment on sulfur K-edge X-ray absorption spectra, Inorg. Chim. Acta, 361 (2008) 956-964.

[72] R.A. Mori, E. Paris, G. Giuli, S.G. Eeckhout, M. Kavcic, M. Zitnik, K. Bucar, L.G.M. Pettersson, P. Glatzel, Electronic Structure of Sulfur Studied by X-ray Absorption and Emission Spectroscopy, Anal. Chem., 81 (2009) 6516-6525.

[73] J.H. Lee, D. Trimm, N.W. Cant, The catalytic combustion of methane and hydrogen sulphide, Catal. Today, 47 (1999) 353-357.

[74] A.T. Gremminger, H.W.P. de Carvalho, R. Popescu, J.-D. Grunwaldt, O. Deutschmann, Influence of gas composition on activity and durability of bimetallic Pd-Pt/Al_2O_3 catalysts for total oxidation of methane, Catal. Today, 258 (2015) 470-480.

[75] A. Datta, R.G. Cavell, R.W. Tower, Z.M. George, Claus Catalysis. 1. Adsorption of SO_2 on the Alumina Catalyst Studied by FTIR and EPR Spectroscopy, J. Phys. Chem., 89 (1985) 443-449.

[76] A. Datta, R.G. Cavell, Claus Catalysis. 2. An FTIR Study of the Adsorption of H_2S on the Alumina Catalyst, J. Phys. Chem., 89 (1985) 450-454.

[77] H. Wijnja, C.P. Schulthess, ATR-FTIR and DRIFT spectroscopy of carbonate species at the aged γ-Al_2O_3/water interface, Spectrochim. Acta, Part A, 55 (1999) 861-872.

[78] G.N. Vayssilov, M. Mihaylov, P. St Petkov, K.I. Hadjiivanov, K.M. Neyman, Reassignment of the Vibrational Spectra of Carbonates, Formates, and Related Surface Species on Ceria: A Combined Density Functional and Infrared Spectroscopy Investigation, J. Phys. Chem. C, 115 (2011) 23435-23454.

[79] C.C. Chang, Infrared studies of SO_2 on γ-alumina, J. Catal., 53 (1978) 374-385.

[80] S.W. Nam, G.R. Gavalas, Adsorption and oxidative adsorption of sulfur dioxide on γ-Alumina, Appl. Catal., 55 (1989) 193-213.

[81] M. Waqif, O. Saur, J.C. Lavalley, S. Perathoner, G. Centi, Nature and Mechanism of Formation of Sulfate Species on Copper Alumina Sorbent Catalysts for SO_2 Removal, J. Phys. Chem., 95 (1991) 4051-4058.

[82] S. Specchia, E. Finocchio, G. Busca, G. Saracco, V. Specchia, Effect of S-compounds on Pd over $LaMnO_3 \cdot 2ZrO_2$ and $CeO_2 \cdot 2ZrO_2$ catalysts for CH_4 combustion, Catal. Today, 143 (2009) 86-93.

[83] E.M. Köck, M. Kogler, T. Bielz, B. Klotzer, S. Penner, In Situ FT-IR Spectroscopic Study of CO_2 and CO Adsorption on Y_2O_3, ZrO_2, and Yttria-Stabilized ZrO_2, J. Phys. Chem. C, 117 (2013) 17666-17673.

[84] P. Bazin, O. Saur, J.C. Lavalley, G. Blanchard, V. Visciglio, O. Touret, Influence of platinum on ceria sulfation, Appl. Catal. B, 13 (1997) 265-274.

[85] M. Waqif, P. Bazin, O. Saur, J.C. Lavalley, G. Blanchard, O. Touret, Study of ceria sulfation, Appl. Catal. B, 11 (1997) 193-205.

[86] M. Waqif, A. Pieplu, O. Saur, J.C. Lavalley, G. Blanchard, Use of CeO_2-Al_2O_3 as a SO_2 sorbent, Solid State Ionics, 95 (1997) 163-167.

[87] S.J. Yang, Y.F. Guo, H.Z. Chang, L. Ma, Y. Peng, Z. Qu, N.Q. Yan, C.Z. Wang, J.H. Li, Novel effect of SO_2 on the SCR reaction over CeO_2: Mechanism and significance, Appl. Catal. B, 136 (2013) 19-28.

[88] G. Liu, J.A. Rodriguez, Z.P. Chang, J. Hrbek, C.H.F. Peden, Adsorption and Reaction of SO_2 on Model $Ce_{1-x}Zr_xO_2$(111) Catalysts, J. Phys. Chem. B, 108 (2004) 2931-2938.

[89] T. Dahmen, P. Rittner, S. Böger-Seidl, R. Gruehn, Thermal Behavior of Sulfates 14. Thermal Behavior of $PdSO_4 \cdot 2\ H_2O$ and $PdSO_4 \cdot 0.75\ H_2O$ and Structure of M-$PdSO_4$, J. Alloy Compd., 216 (1994) 11-19.

[90] J.B. Miller, D.R. Alfonso, B.H. Howard, C.P. O'Brien, B.D. Morreale, Hydrogen Dissociation on Pd_4S Surfaces, J. Phys. Chem. C, 113 (2009) 18800-18806.

[91] L.J. Hoyos, H. Praliaud, M. Primet, Catalytic Combustion of Methane over Palladium Supported on Alumina and Silica in Presence of Hydrogen-Sulfide, Appl. Catal. A, 98 (1993) 125-138.

[92] J.Y. Luo, D. Kisinger, A. Abedi, W.S. Epling, Sulfur release from a model Pt/Al_2O_3 diesel oxidation catalyst: Temperature-programmed and step-response techniques characterization, Appl. Catal. A, 383 (2010) 182-191.

[93] O. Saur, M. Bensitel, A.B.M. Saad, J.C. Lavalley, C.P. Tripp, B.A. Morrow, The Structure and Stability of Sulfated Alumina and Titania, J. Catal., 99 (1986) 104-110.

[94] N.M. Kinnunen, K. Kallinen, T. Maunula, M. Keenan, M. Suvanto, Fundamentals of Sulfate Species in Methane Combustion Catalyst Operation and Regeneration - A Simulated Exhaust Gas Study, Catalysts, 9 (2019) 417.